University of Nairobi

Faculty of Engineering

DEPARTMENT OF GEOSPATIAL AND SPACE TECHNOLOGY

Mapping *Prosopis juliflora* Aboveground Biomass Using Remote Sensing in Taveta Sub-County, Kenya

Rose Njambi Kihungu

F56/38176/2020

A Project Report submitted in partial fulfilment of the requirements for the Degree of Master of Science in Geographic Information Systems, in the Department of Geospatial and Space Technology of the University of Nairobi

August 2022

Declaration

I, Rose Njambi Kihungu, hereby declare that this project report is my original work. To the best of myknowledge, the work presented here has not been presented for a project at any other university.

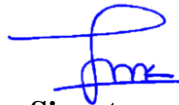Rose Njambi Kihungu   23.08.2022

Name of student   **Signature**   **Date**

This project report has been submitted for examination with my approval as university supervisor

Prof. Faith N. Karanja   23.08.2022

Name of supervisor   **Signature**   **Date**

Acknowledgement

Abstract

Prosopis juliflora is a widespread invasive species listed on the Global Invasive Species Database (GISD) among the 100 most invasive species in the world. Introduced in Kenya in the 1970s–1980s, it has spread rapidly and is now found in 2% of Kenya's landmass (KEFRI, 2020) with the ability to double its coverage every 5 years under favourable conditions (IUCN (International Union for the Conservation of Nature), 2010). *Prosopis juliflora* has negative impacts such as loss of biodiversity, injury to humans and livestock, and loss of livelihood for the affected communities. Its invasive characteristics make it a challenging species to control and eradicate. A *Prosopis juliflora* aboveground biomass map contributes to a better understanding of its spatial distribution and helps to inform control and management approaches.

This study aims to evaluate the suitability of LiDAR point clouds to estimate the aboveground biomass (AGB) of *Prosopis juliflora* and subsequently map its AGB distribution. The AGB of *Prosopis juliflora* in 21 sample field plots were estimated using allometric equations. Regression models were then fitted over the field estimated AGB and LiDAR metrics to identify the significant prediction variables. These were used to model wall-to-wall AGB in the study area. To segregate *Prosopis juliflora* AGB from other vegetation, Sentinel 2 imagery was classified using a random forest binary classification.

The results were a *Prosopis juliflora* AGB map and a predictive model for estimating *Prosopis juliflora* AGB from LiDAR data. The map could help policymakers to develop and implement effective control, management, and utilisation measures targeting areas with the highest biomass. e.g., as outlined by Adoyo et al., (2021). Uncertainties in the obtained results are due to, among others, the choice of allometric equations and classification errors attributable to the mixture of *Prosopis juliflora* with other vegetation species, and the spatial resolution of Sentinel 2 imagery.

Table of Contents

List of Tables

List of Figures

1   INTRODUCTION

1.1   Background

Prosopis juliflora (hereafter simply *Prosopis*) was widely introduced in Kenya in the 1970s to counter the effects of desertification namely tree cover loss, and famine (Choge & Pasiecznik, 2005). Initially, *Prosopis* was appreciated for its benefits (e.g., preventing soil erosion, providing shade, and a source of food for livestock) but over time, the detrimental effects (e.g., rapid spread, forming impenetrable thickets, and thorn injuries) became apparent (Andersson, 2005).

Introduced in dry regions, it has spread to other parts through natural dispersal. *Prosopis* is now a common shrub in the drylands with estimates showing that it makes up to 2% of Kenya's landmass (KEFRI, 2020)

Figure 1-1: Image showing Prosopis (R. Kihungu, Taveta, 30.1.2022)

Being a fast-growing and drought-tolerant species, the invasion of *Prosopis* threatens indigenous plants (Muturi et al., 2010) and causes a decrease in productive land area. Further, their thorns can injure both humans and animals, and their seeds can sometimes lead to the death of livestock. Being a hard species to eradicate, there is a need for control measures that reduce the negative impacts while utilizing it as a resource.

One way is by using *Prosopis* as a source of bio-energy. For this, accurate estimates of biomass are required to quantify the expected energy outputs. Maps of *Prosopis* biomass help to target spatial interventions to areas with the highest bio-energy potential. Furthermore, biomass estimates help to determine the amount of carbon stored and thus *Prosopis* carbon sequestration potential at a time when carbon markets are emerging and could be another source of income.

1.2 Problem Statement

The invasion of *Prosopis* has degraded productive land, reduced local species, and adversely affected communities (Linders et al., 2020). Luckily, the negative social, economic, and ecological impacts associated with its spread can be mitigated if it were to be used as a source of biomass energy. In this regard, there is a need for robust and efficient methods of quantifying the available *Prosopis* biomass. However, studies about using LiDAR data for mapping *Prosopis* biomass were scarce. This study will contribute knowledge to the estimation of *Prosopis* biomass as well as the determination of the relationship between biomass, and LiDAR point clouds (Ku & Popescu, 2019).

1.3 Objectives

The overall objective was to map the aboveground biomass (AGB) of *Prosopis* in Taveta.

The specific objectives were namely to:-

- Identify LiDAR variables with the highest predictive power of *Prosopis* AGB

- Assess the accuracy of different variable combinations in estimating *Prosopis* AGB

- Generate a map of the AGB of *Prosopis* in the study area

1.4 Justification for the Study

Over 75% of Kenyan households are dependent on wood fuel, i.e., firewood and charcoal (Chidumayo & Gumbo, 2010) with 93.2% of rural households using it as their primary fuel source (Ministry of Energy & Clean Cooking Association of Kenya, 2019). The reliance on wood fuel has led to the degradation of forested land. In the face of growing demand for sustainable fuel and calls for the protection of forests, *Prosopis* can help bridge the energy gap by utilization for biofuel production (Witt, 2010).

AGB is defined as "the dry mass of live or dead matter from tree or shrub (woody plant) life forms"(Duncanson et al., 2021). AGB only accounts for biomass above the ground and does not, therefore, include biomass found in the roots (belowground biomass). AGB measurement is important for estimating the carbon stock available for use as bioenergy feedstock that emits less greenhouse gas pollution into the atmosphere than fossil fuels. Further, mapping *Prosopis* biomass provides valuable information for invasive species management, control, and utilization planning.

This study maps *Prosopis* AGB using aerial LiDAR scanning data. It develops a baseline map of *Prosopis* AGB in the study area. The results of this study can inform control and management strategies by governments including projects aiming to utilize *Prosopis* to derive an income. Further, the methodologies and AGB models can be used to map the biomass of *Prosopis* occurring in other areas beyond the scope of this study.

1.5 Scope of Work

This study covers a 58-square-kilometre study area in Taveta, southern Kenya. It involves measurement of stem diameter and height of *Prosopis* occurring in 0.1ha sample field plots; computation of *Prosopis* AGB in the sample plots using allometric equations; development of *Prosopis* AGB estimation models by relating sample plot AGB to LiDAR variables; and classification of *Prosopis* distribution using Sentinel 2 imagery. This study will produce a *Prosopis* AGB distribution map within the study area.

1.6 Organization of the Report

This report is organized into five chapters. Chapter one introduces the topic, gives a background of the study, and outlines the objectives and scope of the project. Chapter two reviews previous literature on the topic. Chapter three focuses on the materials, data, and methods used to conduct the study. Chapter four presents the results achieved and discusses them against previous studies. Finally, chapter five presents the conclusions, and gives recommendations and areas for further research.

2   LITERATURE REVIEW

2.1 Invasive Species Overview

Iannone et al., (2021) define invasive species as "a species that (a) is non-native to a specified geographic area, (b) was introduced by humans (intentionally or unintentionally), and (c) does or can cause environmental or economic harm or harm to humans." Invasive plant species can survive in varied environmental conditions; spread rapidly; and resist pests, predators, or diseases (Ratnayake, 2014), eventually becoming established in an area.

The effects of invasive plant species include but are not limited to competition with indigenous plants for nutrients, water, and sunlight—eventually replacing indigenous vegetation, reduction in productivity of agricultural land, physical injuries to livestock, wildlife, or people, prevention of access to natural resources such as water, and alteration of an ecosystems processes and composition. Ultimately, invasive species lead to socio-economic losses (*Economic and Social Impacts | National Invasive Species Information Center*, n.d.) and increased poverty in the affected communities. Once established and widespread, invasive species become hard to eradicate and their impacts on the natural environment and livelihoods become permanent unless mitigated through ongoing management (Witt & Luke, 2017).

Kenya has many invasive plants within its borders. *Lantana camara* (Lantana)*, Prosopis* (mesquite)*, Opuntia ficus indica*, and *Psidium guajava* are the most prevalent dryland invaders (Obiri, 2011). *Prosopis*, known locally as *Mrashia* (Taveta), is a tree, sometimes shrub, native to South America, Central America, and the Caribbean. The specific origins of the *Prosopis* species found in East Africa are unknown (Pasiecznik et al., 2001). It is one of the most invasive woody species in tropical drylands (Pasiecznik, 2018), and is listed on the Global Invasive Species Database (GISD) among the most invasive species worldwide. *Prosopis* has spread widely having already invaded 2% of Kenya's landmass (1.5 million hectares) (KEFRI, 2020) with the ability to double its coverage every 5 years under favourable conditions (IUCN (International Union for the

Conservation of Nature), 2010). A study by Maundu et al., (2009) found that half the country has a 30%, or more, probability of *Prosopis* invasion.

Prosopis normally grows to a height of 10m but may reach 20m under favourable conditions e.g., areas protected from the wind and with a high water table. The biophysical limits for the growth of *Prosopis* are: altitudes 0-1500 m, mean annual temperature of 14-34º C and mean annual rainfall of 50-1200 mm. The tree/ shrub can grow in a variety of soils including highly saline and rocky soils (World Agroforestry, n.d.). Additionally, *Prosopis* has small dark green leaves (World Agroforestry, n.d.) and an extensive root system which makes it adapted to extreme weather conditions such as high temperatures and low rainfall (Ng et al., 2017). Compared to grass, *Prosopis* pods, though palatable, negatively affect livestock health (Ayanu et al., 2015; Maundu et al., 2009). Consequently, *Prosopis* causes increased pressure on the existing grasslands leading to overgrazing, land degradation, and even conflicts (Linders et al., 2020). Moreover, *Prosopis* has been found to have allelopathic effects on other plant species meaning that it inhibits the growth of other vegetation around it (Ayanu et al., 2015; Pasiecznik et al., 2001).

2.2 History and Impacts of *Prosopis* Invasion in Kenya

In Kenya, *Prosopis* was first planted in 1973 to rehabilitate quarries near Mombasa (Esbenshade & Grainger, 1980). Thereafter, in the 1980s, *Prosopis* was planted on a large scale to reclaim desert land as part of a dryland rehabilitation scheme in the Tana River and Turkana Districts. The scheme was supported by the Food and Agriculture Organization (FAO), and funded by Finland and Norway (Pasiecznik et al., 2008). *Prosopis* was the tree of choice because it is a multipurpose tree that can survive poor soils and harsh environmental conditions—where most other species cannot. The pods are a source of food for livestock, and sometimes, humans. The wood may be used as a source of fuel, for the construction of buildings, or to make furniture (Pasiecznik et al., 2001). Further, the trees can add soil nitrogen and are a source of forage for bees (World Agroforestry, n.d.).

Due to a lack of knowledge of the future risks posed by this species, the first plantations were unmanaged. *Prosopis* quickly spread through dispersal by animals and water, outcompeting and replacing native vegetation, including trees, shrubs, and grass. It is now a major invader in Kenya's

arid and semi-arid lands (ASALs) including Baringo, Bura, Garissa, Mandera, Marsabit, Mwingi, Tana river, Taita Taveta, Turkana, and Wajir counties (*Petition 466 of 2006 - Kenya Law*, 2007).

Initially appreciated for their benefits, over time, the *Prosopis* invasion has led to negative impacts including the loss of grazing land, injuries to both humans and animals, loss of teeth, and eventual death of goats. Additionally, their root system allows them to utilize both surface and groundwater resources, thus lowering the water table (Dzikiti et al., 2013) and increasing the effects of drought (Obiri, 2011). The intended benefits of this invasive shrub have been overshadowed by its negative economic and environmental impacts. While it was introduced to diversify livelihoods, only utilization as a source of wood has proved profitable but even then, this income is cancelled out by a reduction in income from the declining numbers of livestock. Overall, the introduction of *Prosopis* has reduced the resilience of communities to drought (Linders et al., 2020).

Notably, in 2006, harm caused by *Prosopis* to the environment and livelihoods saw the Ilchamus (local community in Baringo County) take legal action against the Government of Kenya (GoK) and FAO (*Petition 466 of 2006 - Kenya Law*, 2007) for introducing the species. They claimed that, among others, *Prosopis* had robbed them of grazing land, caused harm to livestock and humans, blocked roads, and generally, led to huge economic losses. As a result, in 2018, the GoK declared *Prosopis* a noxious weed under the Suppression of Noxious Weeds Act (CAP 325) (*Kenya Law: CXI No. 2 - 9th January 2009*, 2009).

It is important to point out that in some regions of the world, such as Sudan (Laxen, 2007) and India (Walter, 2011), the benefits from the utilisation of *Prosopis* have outweighed the costs, with the species even considered sacred in parts of India. The problem in Kenya, therefore, may be a lack of knowledge on proper management (*Prosopis* does not become weedy when properly managed), or the introduction of poor genetic *Prosopis* which is shrubby and has limited value (Pasiecznik et al., 2001).

2.3 Combating the *Prosopis* Invasion

Once they are well established, preventing the further spread of *Prosopis* is currently deemed impossible (Pasiecznik, 2018). This is because its seeds spread easily and remain viable for at least 40 years. Water flow during the rainy season or flooding events facilitates its widespread dispersal, which is made worse by animals that feed on *Prosopis* pods and thereafter excrete the seeds in different environments.

Measures to stop the further spread of *Prosopis* may entail manual or mechanical control by uprooting all the identified trees. However, this method is labour-intensive and expensive, not to mention the risks posed by the thorns to the workers involved. In Kenya, Maundu et al., (2009) estimated the average cost of clearing *Prosopis* to be US$227,000 per sq. km (as of 2009). With an estimated area of 1.5 million hectares (KEFRI, 2020) suspected to be under *Prosopis.* invasion, manual clearing would be an expensive endeavour. Further, uprooting *Prosopis* trees on a large scale would likely lead to the destruction of the surrounding non-invasive vegetation, or leave the soils bare, leading to degradation.

Chemical control by the application of herbicides is another method of controlling the spread of *Prosopis.* Using this method alone, however, is expensive and only effective in restricted zones as opposed to large tracts of invaded land. In Kenya, *Prosopis* mostly exists in extensive tracts of unrestricted lands, making this method unfeasible. Further, the widespread use of chemicals may pose negative environmental and health effects (Pasiecznik, 2018).

Biological control measures using host-specific insects, mites, or pathogens are an alternative measure that can be employed to control the spread of *Prosopis.* This method has mostly been practised in Australia and South Africa. In Australia, it has been more successful (Shackleton et al., 2014) than in South Africa (Wilgen et al., 2012; Zachariades et al., 2011) where it has been ineffective at stopping the invasion (Wise et al., 2012). While biological methods are suitable for expansive areas, they are not widely practised because they may harm native species (Pasiecznik, 2018), and are expensive to implement (Shackleton et al., 2014).

Though mechanical, chemical, and biological attempts to eradicate *Prosopis* species continue in different parts of the world, these have largely been unsuccessful (Pasiecznik, 2018). There is a growing consensus that a more feasible method is through utilization for the socio-economic benefit of the community: a method known as control through utilization (Shackleton et al., 2014). The downside to this method is: (a) encouraging utilization may lead to dependency and hence conflict of interest with the goal of eradication, and (b) areas with poor quality species that are weedy and thorny will have limited utility (Shackleton et al., 2014). Moreover, the decision to utilise *Prosopis* depends on factors such as its location, economic profitability, and people's knowledge and perceptions. People's knowledge and perceptions are, in turn, determined by its effect on the people's livelihoods. For instance, pastoralists are more likely to support total eradication owing to its harm to their livestock and grazing land while farmers in marginal lands—where irrigation is impossible—might choose to grow it for charcoal production or other valuable wood products (Ayanu et al., 2015; Pasiecznik et al., 2008; Wakie et al., 2016).

In Kenya, the question of eradication or control through utilization is still an ongoing debate (Maundu et al., 2009). In the past, the government has launched initiatives to educate communities and build their capacity to realize the full potential of *Prosopis* (KEFRI, 2020; Pasiecznik et al., 2006; Tuwei et al., 2019). The main utilization methods proposed are charcoal production, pods for animal feed and as human food, and energy generation (KEFRI, 2020). Today, charcoal production from *Prosopis* is the most common way of utilizing these stands as it requires little initial capital and yields high returns. In Baringo County, the annual income from *Prosopis* charcoal is approximated to be 11 million Kenyan shillings (KEFRI, 2020). That said, in Kenya, *Prosopis* remains underutilized due to a deficiency of suitable knowledge and investment in research and development of the most suitable technologies for harvesting and processing (Pasiecznik et al., 2015).

There is still no evidence, however, that control through utilization is a successful method for reducing *Prosopis* invasions (Shackleton et al., 2014). On the contrary, Mbaabu et al., (2019) found that control through utilization furthers the spread of *Prosopis*. A finding supported by Linders et al., (2020) and Ayanu et al., (2015) who conclude that when cut, *Prosopis* quickly coppices resulting in more cover and smaller stems which are less suitable for fuelwood. Mbaabu

et al., (2019) and Linders et al., (2020) recommend the replacement of *Prosopis* with native trees (which have higher quality wood) and grasslands after cutting down. It is worth pointing out that while *Prosopis* helps lower the amount of carbon dioxide (CO_2) in the atmosphere, the replacement of degraded grasslands with *Prosopis* is not a good solution as it leads to severe environmental and socio-economic problems. Healthy grasslands, on the other hand, can store as much, or even more, soil organic carbon than *Prosopis* (Mbaabu et al., 2020). Generally, countries with large-scale *Prosopis* invasions integrate different control and management methods (Mbaabu et al., 2019; Shackleton et al., 2014).

2.4 Remote Sensing for *Prosopis* Mapping

Given the spatial-temporal variation in *Prosopis* invasions, spatially explicit management and control approaches customized to different invasion rates, scales, and socio-economic conditions would ensure greater success (Adoyo et al., 2021). To this end, accurate maps of its spatial distribution and quantity (AGB) are needed to aid in the identification of hotspots; determination of priority areas; monitoring whether control measures applied are working and predicting spread. Remote sensing technologies provide information on *Prosopis* extent (through land use and land cover classification) and carbon densities (through aboveground biomass mapping) (Amara et al., 2020).

Remote sensing collects data on an object without coming into contact with the object (International Organization for Standardization (ISO), 2016). Sensors can be installed on the ground, on airborne platforms such as aeroplanes and drones, or spaceborne platforms like satellites. Remote sensing data is essential for the detection and estimation of variables related to invasive species such as distribution, density, and impacts (Huang & Asner, 2009).

Several factors make remote sensing an efficient tool for invasive species mapping. First, invasive species often spread quickly to occupy large tracts of land. Remote sensing enables large-scale mapping and monitoring which would not be possible otherwise. Second, the high temporal resolution of remote sensing sensors enables regular monitoring of invasive species. Third, remote sensing allows for direct measurement of plant characteristics, e.g., crown width and height, in remote, vast, and inaccessible areas where fieldwork is unfeasible. The detected plant

characteristics can then be extended for the measurement of other characteristics such as biomass. Finally, remote sensing provides long-term archives which can be utilized to map and monitor the spread of invasive species.

2.4.1 Optical Remote Sensing for *Prosopis* Mapping

Several optical sensing systems have been used to study the distribution of *Prosopis*. Specifically, archive imagery collected by Landsat satellites since the 1970s (Garner, 2015) has been extensively utilised in Africa. In Somalia, Tilahun & Asfaw, (2012) modelled the expansion rate of *Prosopis* using Landsat ETM+ satellite imagery. Rembold et al., (2015) mapped the national scale *Prosopis* invasion in Somaliland using Landsat 8 imagery in conjunction with ground observation data. They used probability thresholds on a maximum likelihood classifier to determine the presence or absence of *Prosopis*. *Prosopis* distribution mapping in West Somaliland using a combination of Landsat 8 imagery, ground truth data, and spectral measurements was undertaken by Meroni et al., (2017). They used random forest classification on imagery acquired at different times (wet season, dry season and a combination of the two) and different spatial resolutions (30m original imagery and 15m pansharpened imagery). The combination of wet and dry season images performed slightly better than dry season images while pansharpening minimally increased accuracy.   In Ethiopia, Ayanu et al., (2015) analyzed the spread of *Prosopis* from 2000 to 2013 using Landsat ETM+ and ASTER imagery while Haregeweyn et al., (2013) used Landsat imagery to analyse the invasion rate in Amibara District from 1973 to 2004. Berg et al., (2013) used multiresolution satellite imagery, i.e., Landsat and MODIS, to map the extent, canopy density, spreading trends, and areas susceptible to invasion of *Prosopis* in South Africa. The invasion of *Prosopis* in Sudan's Kassala plain was studied by Hoshino et al., (2012) using Landsat TM imagery for species detection and distribution and PALSAR radar data to examine their effect on soil moisture content. In Kenya, Muturi et al., (2010) used Landsat imagery and field data to estimate *Prosopis* invasion trends in the Turkwel Riverine Forest ecosystem (Turkana County) between 1995 and 2006. Mbaabu et al., (2019) used multispectral, multitemporal and bi-seasonal Landsat images to study the spatial trends of *Prosopis* in Marigat and their impacts on land cover and livelihoods.

Designed to build a virtual constellation with Landsat (Wulder et al., 2015), the launch of the Copernicus Sentinel 2 mission in 2015 avails high temporal, spatial, and spectral resolution imagery, further facilitating studies on the spread and distribution of *Prosopis*. Ng et al., (2016) used Sentinel 2 data to detect and map *Prosopis* in the Tarach water basin, Turkana, Kenya using the same classification scheme as Rembold et al., (2015). They used dry season image bands and applied a random forest classifier in the R environment. Besides the raster bands, they also input the Normalized Difference Vegetation Index (NDVI) and an elevation model to improve the classification results. They reported a 99% classification accuracy which they contend might be lower due to the lack of a separate validation dataset. In Ethiopia, Ahmed et al., (2021) evaluated the performance of various invasive species distribution predictive models (e.g., random forest, support vector machine and generalized additive model) using Sentinel 2-derived radiometric indices and biophysical variables. Specifically, they evaluated model performance when applied to predicting *Prosopis* distribution. The performance of the random forest model was very high highlighting its importance in invasive species distribution prediction. In Marigat sub-County, Baringo, Kenya, object-oriented random forest *Prosopis* classification using Sentinel 2 and Pléiades imagery was undertaken by Ng et al., (2017). In addition to the image bands, they also used vegetation indices and texture information to improve the classification. They found that while higher spatial resolution Pléiades imagery enables classification at a higher level of detail, the higher spectral resolution of Sentinel 2 imagery enables better detection and differentiation of different vegetation types.

Within Taita Taveta County, Kenya, few attempts have been made to study the *Prosopis* invasion using remote sensing data. Maundu et al., (2009) mapped *Prosopis* distribution in Kenya using information obtained from herbarium specimens and field data. They found that Tsavo National Park (located in Taita Taveta County) was one of the areas facing rapid *Prosopis* invasion facilitated by animal droppings as pastoralists traversed the area in search of pasture. This study utilized field data and not remote sensing techniques. Muturi, et al., (2012) focused on the distribution of *Prosopis* species in Kenya. In addition to noting that Taveta was under intermediate threat of invasion, they found that *Prosopis Chilensis* was the most likely *Prosopis* species in Taveta and not *Prosopis juliflora* as earlier thought. Other research looked into the

commercialization of *Prosopis* products (KEFRI, 2020). However, mapping of *Prosopis* biomass using remote sensing techniques has not been achieved for Taveta.

2.4.2 LiDAR for AGB Estimation

Light Detection and Ranging (LiDAR) is an active remote sensing method which utilizes a laser scanner to emit light as a transmitted laser to target objects on the Earth's surface and record the reflected signals. In this way, it measures ranges (distances) from the sensor to the target objects. The resulting LiDAR point cloud data are used to create 3-dimensional elevation models and for depicting vegetation structure which is useful for extracting characteristics like tree height, diameter, and crown width (Ku & Popescu, 2019). The use of LiDAR sensors installed on an airborne platform such as an aircraft is known as Airborne Laser Scanning (ALS) (Hansen et al., 2015).

ALS has emerged as an accurate method for aboveground biomass estimation, producing better results than radar and optical remote sensing methods (Zolkos et al., 2013). AGB estimation using ALS is normally done through a combination of field sampling, allometric models, and LiDAR metrics (Zolkos et al., 2013). This is usually a three-stage procedure. First, allometric models are used to compute sample field plot biomass. Second, sample plots are used to derive relationships between ALS metrics and tree characteristics measured in the field. Finally, such relationships are used to compute AGB estimates from ALS data (Næsset, 2002).

Although still inconclusive, in some cases, combining optical, radar, and LiDAR sensors leads to more accurate AGB models whose values are closest to field observations (Zolkos et al., 2013). The integration of LiDAR and aerial imagery has been used to derive biomass maps for multiple vegetation types like multi-use savannah landscapes (Amara et al., 2020), forest landscapes (Chen et al., 2012), and dense tropical submontane rainforests (Hansen et al., 2015). Contrary to other studies, (Zhao et al., 2021) found that high-resolution multi-spectral imagery performed better than LiDAR. It should be noted however that this study used UAV-LiDAR as opposed to ALS.

2.4.2.1 LiDAR Models Used in AGB Estimation and Accuracy Assessment

LiDAR metrics describe the distribution of trees in a stand and are important for AGB estimation. Examples of ALS variables commonly used to predict biomass are canopy height metrics such as mean, median and skewness, canopy density variables, LiDAR return characteristics, etc. (Chen et al., 2012; Hansen et al., 2015). Generally, ALS variables used to predict biomass vary depending on the vegetation type: canopy density variables in dense tropical submontane rainforests (Hansen et al., 2015), laser penetration variables in tropical lowland forests (Phua et al., 2017), median height of the LiDAR canopy model for tall, high biomass, tropical forests (Réjou-Méchain et al., 2015).

(Ku & Popescu, 2019) applied both LiDAR data and aerial imagery in comparing different methods of estimating *Prosopis* AGB. They found that in addition to a raster CHM, the maximum height was important to the determination of *Prosopis* AGB. Amara et al., (2020) extracted height and canopy cover metrics—at a 3.5m threshold—for the determination of the AGB of woody plants in a Kenyan savannah. A two-variable LiDAR model was found optimal for AGB estimation whereby the predictors used were the percentage of all returns above 3.5 m and the minimum elevation of the first returns above 3.5 m. LiDAR return height distribution and canopy cover variables extracted by (Heiskanen et al., 2019) in an Afromontane landscape were found significant for AGB estimation. More specifically, they found that a two-variable model containing canopy cover and density metrics and canopy height was the most optimal for AGB prediction in a non-stratified forest environment.

It is important to evaluate LiDAR AGB models to ensure the accuracy of predicted AGB values (Valbuena et al., 2017). Various methods are applied in assessing and selecting the optimal LiDAR AGB model. Regression models fit between LiDAR variables and field plot AGB estimates are used to show which relationships are significant and the nature of these relationships. The null hypothesis is that there is no relationship between the LiDAR variable and field plot AGB. One of the results of regression analysis is the p-value. This is used to assess whether the LiDAR variable is significant or not. A p-value less than the significance level means that the null hypothesis is false and the LiDAR variable is significant.

Where there is no independent dataset for the accuracy assessment of regression equations, cross-validation is usually used (Næsset, 2002). Cross-validation entails the removal of one dataset at a time and fitting the model to the remaining datasets. The fitted model is then used to predict the removed dataset. Leave-one-out cross-validation (LOOCV) accuracy statistics such as mean difference, root mean square error (RMSE), pseudo coefficient of determination (R^2), and mean absolute difference can then be used to assess the prediction methods. (Amara et al., 2020; Heiskanen et al., 2019). Additionally, regressing predicted AGB as the independent variable (x-axis) against observed AGB as the dependent variable (y-axis) and checking whether these follow the 1:1 line can also be used for model assessment (Valbuena et al., 2017).

2.4.2.2 Uncertainty in LiDAR AGB Estimation

LiDAR AGB estimates usually involve using field measurements to calibrate the remote sensing data. Even though LiDAR AGB modelling results can be relatively accurate, AGB estimates are not free of errors. The errors arise from uncertainties involved during various steps. One source of error is the measurement of sample tree heights in areas with dense canopies. It is not only difficult to distinguish the highest point on a specific tree but also one may be forced to stand close to the tree when measuring the height using a clinometer as opposed to the recommended distance away from the base of the tree. Besides, but related to height measurement, another source of error is the selection of a height-diameter (HD) model to infer the heights of trees whose height was not measured directly in the field. Here, variations may occur depending on the HD model used. Developing local HD models as opposed to using generic models may reduce this error (Réjou-Méchain et al., 2017).

Sample sizes are another source of uncertainty. ALS model errors usually decrease with increasing sample sizes because they are less affected by edge effects and GPS positioning errors (Zolkos et al., 2013). Edge effects can however be mitigated by using circular plots which have a smaller circumference to area ratio. That said, it is difficult to establish large field plots in areas with dense vegetation or rugged terrain. Further, larger plots increase the inventory costs. Thus, there is a need for a cost-benefit analysis to balance precision and costs(Næsset, 2002). The size of field observation plots in the tropics usually ranges between 0.1 and 1.0 ha (Hansen et al., 2015) with the minimum plot size dependent on the type of LiDAR used (Zolkos et al., 2013).

Another source of error is the choice of the AGB allometric model. The accuracy of estimated biomass is dependent on the underlying accuracy of the allometric models used to extrapolate ground estimates to LiDAR metrics (Chave et al., 2004; Duncanson et al., 2017). In turn, the accuracies of allometric models depend on the sample sizes, their spatial distribution, and the environmental conditions of the sample areas (Duncanson et al., 2017). Specifically, the development of shrub allometric models calls for greater sample sizes because they are characterized by irregular shapes resulting in varying biomass for a given stem diameter (Roxburgh et al., 2015). Generally, locally derived species-specific allometric equations are preferred because they are perceived to be more accurate than regional, generalized allometric models (Duncanson et al., 2017; Roxburgh et al., 2015). Nevertheless, Roxburgh et al., (2015) point out that using a generic model—like those developed by Chave et al., (2014) which are applicable across the tropics (Duncanson et al., 2017)—may yield acceptable results while outperforming species-specific models in terms of cost-effectiveness and applicability to a wide range of species.

In field plots where the tree stands have achieved maximum height, LiDAR-derived canopy height models have less explanatory power on AGB and may instead underestimate biomass in such field plots (Hansen et al., 2015). According to (Duncanson et al., 2017), this may be addressed by creating allometric models based on terrestrial laser scanning data, which estimates individual tree volumes as opposed to traditional field sampling of diameters and heights.

Finally, diameter measurement errors, uncertainty in wood density values, and coregistration errors between the LiDAR point cloud and sample field plot positions may further contribute to uncertainty in AGB estimates. According to Réjou-Méchain et al., (2017), the choice of allometric model is the main contributor to AGB error, followed by the choice of HD model.

2.5 Allometric Models for *Prosopis* AGB Estimation

Direct harvesting and weighing of individual shrubs or trees is the most exact method of biomass estimation. However, such estimation methods are destructive, time and labour-consuming, and impracticable for extensive or remote areas. Indirect estimation using allometric models is,

therefore, often used whereby representative samples are harvested and weighed, and their AGB is related to easily measured attributes like stem diameter and height. Although their initial development and validation can be expensive, allometric models are an efficient and cost-effective method for large-scale estimation of AGB in new sites when constructing new allometric models is not possible (Duncanson et al., 2021; Roxburgh et al., 2015).

In Kenya, several allometric models exist for *Prosopis* biomass estimation. Maghembe et al., (1983) estimated *Prosopis* biomass in one of the earliest *Prosopis* plantations in the country. They sampled eleven 6-year-old *Prosopis* trees grown under plantation conditions. Sample diameters ranged from 4.9 cm to 31.7 cm with heights ranging between 7.1m and 19.7 m. The result was four linear allometric equations for predicting the biomass of tree components namely the leaves, stem, large branches and small branches. The total biomass is the sum of these components. Allometric models for estimation of *Prosopis* in naturally occurring stands were computed by Muturi et al., (2012) through destructive sampling. The field plots were 0.1ha in size and located in arid areas of Katilu, and Nadapal, with additional sites in Marigat and Bura, used for validation. With Taveta also being an arid area, these allometric models could be used for AGB estimation.

However, some differences are noted. First, the Nadapal site is located in a riverine site with a microclimate that could be significantly different from the Taveta study site. Second, the basal diameter (D30) range of the trees used to develop the model was between 2.6cm and 18.5cm. The Taveta study site, on the other hand, has significantly bigger *Prosopis* trees with basal diameters of up to 73.2cm. According to (Duncanson et al., 2017, 2021), extrapolating beyond the limits of the sample diameters used to create the allometric model could introduce bias. Additionally, differences in the frequency distribution of tree sizes used in the construction of allometric models and the sample increase uncertainty in the estimated biomass (Roxburgh et al., 2015). Lastly, most *Prosopis* tree samples used in the allometric model development branched above D30 whereas for the Taveta samples, most trees branch below D30.

The recommended equation by Muturi et al., (2012) shows a logarithmic linear relationship between basal diameter and *Prosopis* biomass. To compute *Prosopis* AGB, Linders et al., (2020) modified this equation into a power model which they hypothesized fit the data from Muturi et al., (2012) best. *Prosopis* is mostly a multi-stemmed plant (Maghembe et al., 1983). Muturi et al., (2012) did not explore the effect this has on the allometric model. Kyuma et al., (2018) sought to fill this gap by destructively sampling 128 trees. They developed power and curvilinear allometric models for estimating the biomass of multi-stemmed *Prosopis* trees. The study, however, does not explore allometric models for *Prosopis* trees with over three stems. Further, the study does not show the diameter-height distribution of the samples used in model construction.

3 MATERIALS AND METHODS

3.1 Study Area

The study site is a 58 sq. km area located in the Taveta sub-county approximately 100 km from Voi on the Voi-Taveta-Arusha (A23) road. The study site falls within Taita Taveta County which is considered an arid and semi-arid (ASAL) region. The County can be divided into three zones: the highlands or mountainous areas of Taita hills, Taveta at the foot slopes of Mount Kilimanjaro (the location of our study area), and the lowlands which comprise Tsavo National Parks and rangelands. Taveta experiences two rainy seasons occurring in March-June and October-December with an average annual rainfall of 350nm-750nm and temperatures ranging between 21-38°C (NEMA, n.d.).
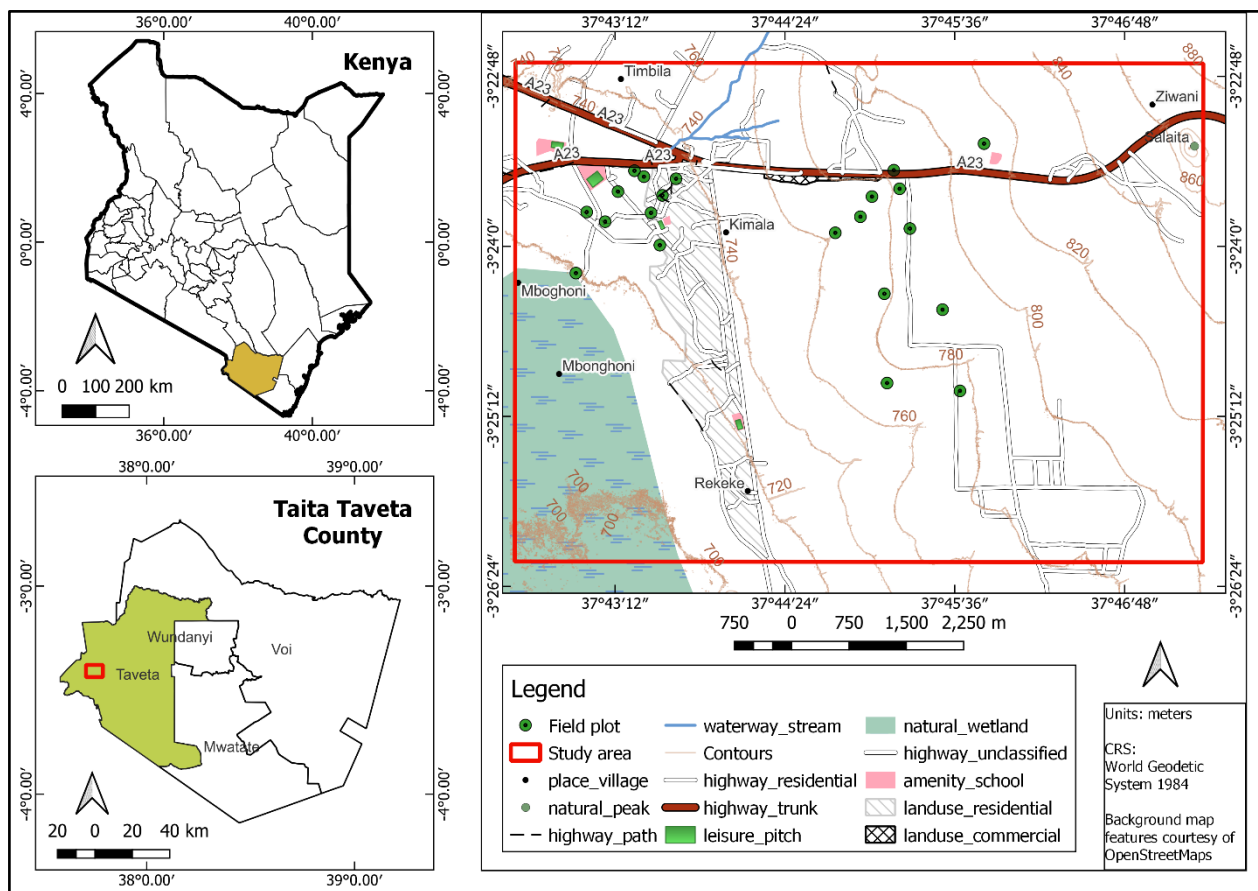
Figure 3-1: Overview of the study area. The red outer bound shows the extent of the 58 sq. km study area while the green dots show the sample plots.

The site is mainly covered by ASAL vegetation of grasslands, woodlands, and shrublands, with savannah species like *Acacia* sp. found in areas with a high water table. Over 90% of Taveta's rural population use firewood while the rest use kerosene and (or) charcoal. The demand for fuelwood (firewood and charcoal) is approximated to be 41,000 tonnes annually leading to deforestation and increasing fuelwood prices (NEMA, n.d.).

3.2 Data Sources and Tools

3.2.1 Data Sources

These include:

- Field plot sample data

- Aerial imagery and LiDAR data

- Sentinel 2 imagery

Table 3-1: Sentinel 2 image bands used in this study

Band	Central Wavelength (nm)	Resolution (m)
Band 1 – Coastal aerosol	443	60
Band 2 – Blue	490	10
Band 3 – Green	560	10
Band 4 – Red	665	10
Band 5 – Vegetation Red Edge	705	20
Band 6 – Vegetation Red Edge	740	20
Band 7 – Vegetation Red Edge	783	20
Band 8 – Near InfraRed	842	10
Band 8a – Vegetation Red Edge	865	20
Band 11 – Short Wave InfraRed	1610	20
Band 12 – Short Wave InfraRed	2190	20

3.2.2 Tools

Activity	Tools
Orientation and recording of field observations	• Handheld GPS • Digital map e.g., Google Maps • Field forms
Establishment of the sample plots	• GNSS base and rover • Measurement tape (30 m) • Compass • Metallic pegs to mark plot centre points
Measurement of diameter and tree height	• Callipers • Levelling staff for tree heights of up to 5m • Hypsometer for tree heights above 5m
Photographic recording	• Digital camera, or phone with a camera

3.2.3 Data Collection

3.2.3.1 Field Plot Measurements

Field data for 21 circular sample plots were collected during the dry season between January and March 2022. *Prosopis* occurs in various forms ranging from large trees with a single stem to multi-stemmed trees to a shrubby form, as shown in **Error! Reference source not found.**. Apart from size, *Prosopis* canopy structure varies from dense to sparse. The plots were selected subjectively to encompass variation in the density and size of *Prosopis* in the study area—which explains the irregular distribution of the sample plots (Figure 3-1).
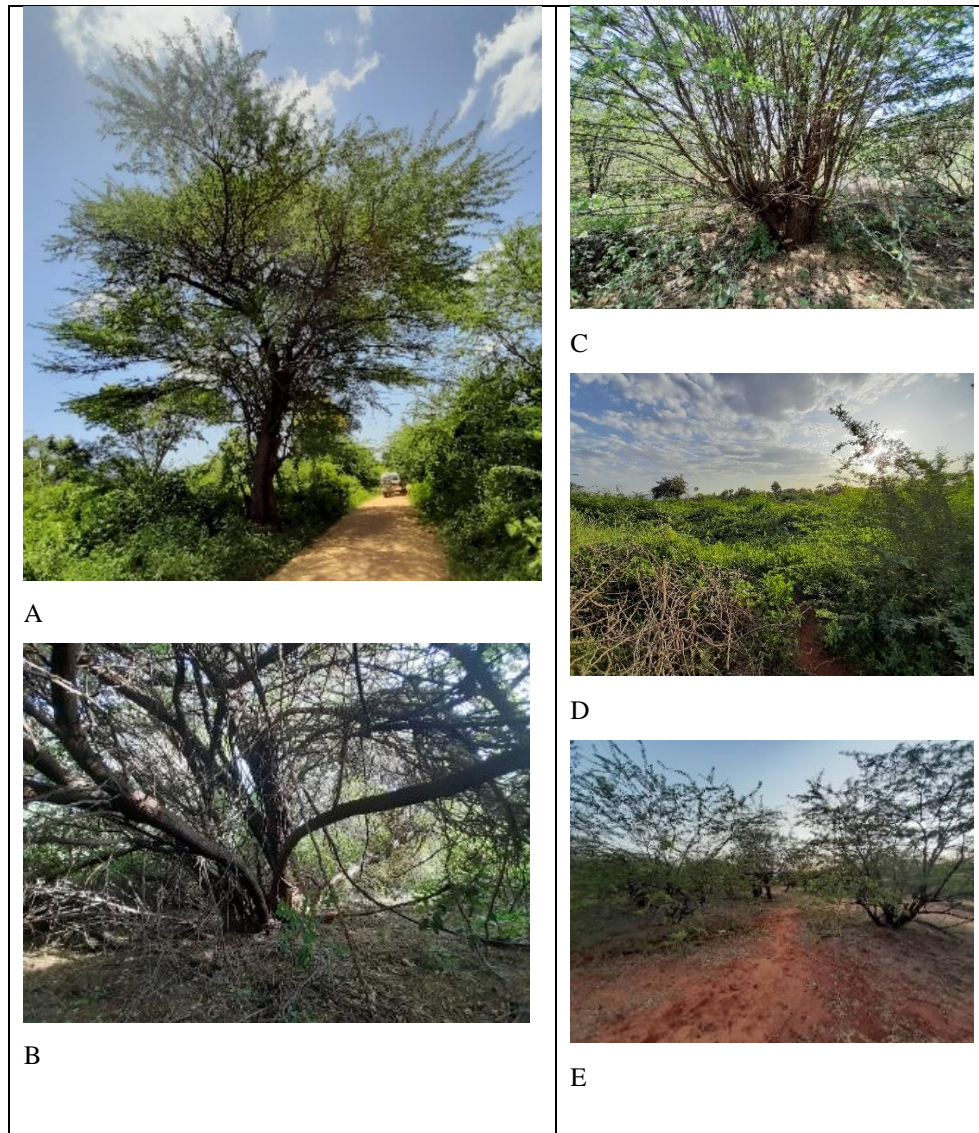
Figure 3-2: Examples of Prosopis forms encountered in the field. (A) Tree with large main stem; (B) multi-stemmed tree; (C) coppiced tree; (D) dense shrubs; (E) sparse shrubs (R. Kihungu, March 2022)

A sample plot comprised a main plot of 0.1ha in size (17.84m radius) and four subplots of 0.01 ha (5.64m radius) following the Land Degradation and Surveillance (LSDF) sample plot design (Figure 3-2). A similar plot layout has been used in earlier studies in the region (e.g., Amara et al., 2020).
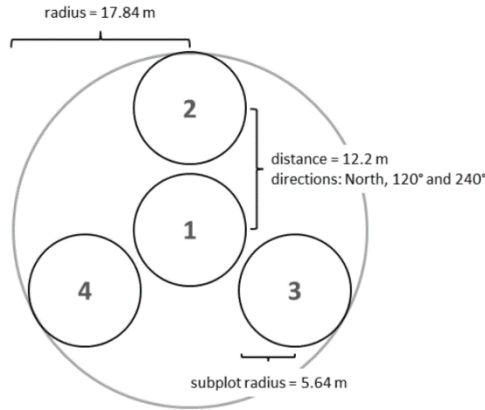
Figure 3-3: Image showing the field plot layouts (Heiskanen et al., 2013)

The centre of the main plot is positioned using differential Global Navigation Satellite System (dGNSS) measurements using a base station on a known point and a rover at the centre of each field plot. The data was recorded for over 30 minutes with a logging rate of 1 second. The antenna height was approximately 3.0 m for most plot centre points. Trimble GPS Pathfinder software was used to post-process centre point coordinates. The maximum standard deviation of the collected measurements was 0.6 metres. The computed centre point coordinates were used to register the plots. 17.84 m buffers were created around the centre points corresponding to circular plots of size 0.1ha.

Within the main plot, basal stem diameter was measured at 30cm height from the ground (D30) using a calliper or tape. Trees with a diameter >= 10cm were identified and their stem diameter and species were recorded. The diameter at breast height (DBH, 1.3 m from the ground) was also measured for trees with D30>=18cm or any other species other than *Prosopis*. The height of trees with the minimum, median, and maximum D30 in the main plot was measured and recorded. Height was measured using a 5 m levelling staff held vertically and read to the highest point of the tree. The height of trees exceeding 5 m was measured using a Suunto hypsometer.

Within the subplots shrubs with a D30 of between 2.5cm and 10cm were counted (for both *Prosopis* and other species). Here, height and D30 were only measured and recorded for the median shrub. The dominant species was recorded and any other species were noted. Other characteristics such as dead trees, dense vegetation, deforestation, charcoal burning, etc., observed

within the field plots were also recorded. Here, woody vegetation with D30>=10cm are called trees.

Table 3-3: Summary of tree and shrub field plot data collected

Summary of Plot Data										
	No. of stems	D30 (cm)			DBH (cm)			H (m)		
		Min	Mean	Max	Min	Mean	Max	Min	Mean	Max
Trees D30 ≥10 cm	557	10.00	16.22	73.20	4.70	12.78	75.10	3.60	7.76	18.00
Shrubs (2.5cm≤D30<10cm)	1310	2.50	4.96	9.00	NA	NA	NA	1.80	4.58	13.00

3.2.3.2 LiDAR and RGB-NIR Data

LiDAR and red, green, blue and near-infrared (RGB-NIR) imagery were collected concurrently on 17th February 2022 during the dry season. The imagery and LiDAR data were collected using Leica RCD30 and Leica ALS60 sensors, respectively mounted on a Cessna aircraft. The point density was approximately 3 points/sq.m.

This data was collected by Ramani Geosystems, Kenya, in conjunction with the University of Helsinki. LiDAR point cloud bare earth points were identified and used to create a digital terrain model (DTM). Relative height values above the ground were obtained by subtracting the DTM from the LiDAR point cloud. In vegetated areas, this relative height can be considered as the canopy height while in open areas and gaps between vegetation, the height is close to zero and hence represents the bare earth (Næsset, 2002). One of the challenges in mapping the bare earth in vegetated areas is that the number of LiDAR ground points affects the accuracy of the DTM and hence the extracted CHM (Réjou-Méchain et al., 2015). As such, extra flight lines were included in the areas with sample plots to maximize increased ground hits. The RGB-NIR imagery was orthorectified and had a spatial resolution of 0.1 m. All datasets were projected in UTM 37South, on WGS84 ellipsoid.

3.2.3.3 Sentinel-2 Imagery

European Space Agency's (ESA) Sentinel-2 mission provides open access to earth observation data at a high spatial as well as temporal resolution (Ng et al., 2017). Sentinel-2 constellation comprises two satellites i.e., Sentinel-2A and Sentinel 2B with approximately 5 days revisit time. Each satellite has 13 bands ranging from the visible to the short-wave infrared portion of the electromagnetic spectrum with a maximum spatial resolution of 10m (*Sentinel-2 - Missions - Sentinel Online - Sentinel Online*, n.d.). In this study, data acquired between March 2021 to March 2022 were used.

3.2.3.4 Classification Training Data

Training data for classification of *Prosopis* invaded areas consisted of field plot locations and additional sites extracted from 10cm spatial resolution aerial imagery. It was necessary to complement the field plot data with photo-interpreted polygons to increase the size of the training data. Training data was selected such that only areas with pure stands and dense *Prosopis* cover were used. This was done to reduce the effects of mixed pixels on the classification. Sites digitized from high-resolution aerial imagery were informed by observations during fieldwork. Aside from *Prosopis* invaded areas, polygons covering different LULC classes were also digitized (Table 3-5).

Table 3-4: Land use land cover (LULC) classes in the study area

ID	LULC	Description
1	Agricultural/ Mixed Vegetation	A combination of crops, trees, shrubs, etc., that exist in a stand.
2	Bare land	Areas with little or no vegetation (exposed soil)
3	Builtup	Areas with human settlements
4	*Prosopis*	Areas invaded by *Prosopis*
5	Tarmac	Tarmac road

The training data were digitized in Quantum GIS (QGIS) and consisted of 71 spatial polygons indicating the presence or absence of *Prosopis* and the LULC class.

Table 3-5: Extract of training data attribute table

fid	class	*Prosopis*
1	*Prosopis*	TRUE
2	*Prosopis*	TRUE
3	*Prosopis*	TRUE
4	*Prosopis*	TRUE
5	*Prosopis*	TRUE
6	*Prosopis*	TRUE
7	*Prosopis*	TRUE
8	*Prosopis*	TRUE
9	*Prosopis*	TRUE
10	*Prosopis*	TRUE
11	Tarmac	FALSE
12	Tarmac	FALSE
13	Tarmac	FALSE
14	Bare	FALSE

3.3 Aboveground Biomass Estimation

3.3.1 Estimating Field Plot AGB

Sample plot *Prosopis* AGB was first computed using the species-specific allometric equation by Muturi et al., (2012):

$$Ln\,(AGB) = \ 0.2933D30 - 0.03$$

(3.1)

However, this equation was found to overestimate AGB heavily outside the range of D30 values used when the model was developed. Kyuma et al., (2018) also found that predictions from this model do not match field observations. Therefore, other allometric equations from previous literature were used to estimate AGB depending on the stem diameter and species.

For *Prosopis* trees and shrubs with D30<18.5 cm, an allometric equation by Linders et al., (2020) which is based on data from Muturi et al., (2012) was used:

$$Ln\,(AGB) = -10.672 + 8.71 \times D30{\char`\^}0.2$$

(3.2)

AGB of *Prosopis* trees with D30≥18.5 cm, and other tree species D30≥10 cm was estimated using (Chave et al., 2014) equation 4:

$$AGB = 0.0673 \times (\rho \times DBH{\char`\^}2 \times H)\,{\char`\^}0.976$$

(3.3)

Other shrub species with D30 between 2.5 cm and 10cm, Conti et al., (2019):

$$AGB = exp(-2.869 + 2.584 \times Ln\,(D30))$$

(3.4)

Where:

AGB = Above-ground biomass in kilograms (kg)

D30 = Diameter measured 30cm from the ground (cm)

ρ = Species-specific wood density (g/cm3)

DBH = Diameter measured 1.3m from the ground (cm)

H = Height (m)

DBH, tree height (H), and species-specific wood density (ρ) are required for equation 3.1. Since DBH was only measured for sample trees, their average DBH/D30 ratio was used to estimate DBH for all trees with D30>=10cm. An average DBH/D30 ratio of 0.844 was used. To infer the height of trees that were not directly measured, sample trees D30 and H were used to fit a local height-diameter model by employing the modelHD function in the R BIOMASS package (Réjou-Méchain et al., 2017).

ModelHD fits four different models to the data and outputs the residual standard error (RSE), average bias, and the residual standard error of the log models as shown in Table 3-6 below.

Table 3-6: Tree height modelling results based modelHD function.

Model	RSE	RSElog	Average_bias
1. log1	2.761864	0.3309373	0.000802307
2. log2	2.789708	0.333839	0.002379401
3. weibull	2.813087	NA	0.02961977
4. michaelis	2.862254	NA	-0.026231735

Log 1 model was selected because it had the highest accuracy (lowest root square error (RSE)) and minimum average bias. Figure 3-4 compares the different models and also shows the selected model.
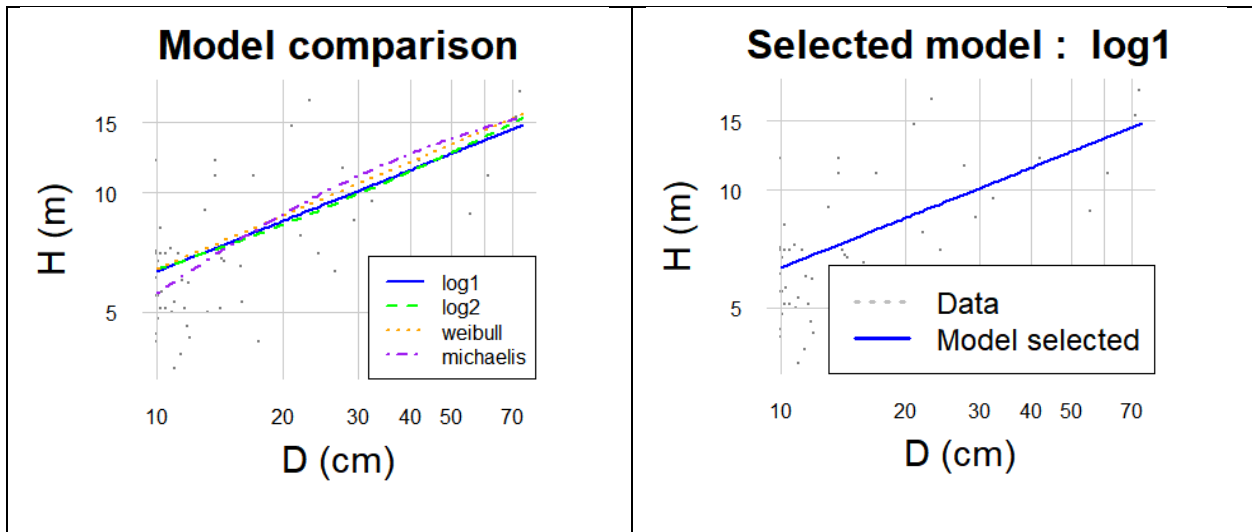
Figure 3-4: Comparison of different HD models (left) and the selected log 1 model (right)

Species-specific wood density was retrieved using the 'getWoodDensity' function in the R BIOMASS package (Réjou-Méchain et al., 2017). The function estimates wood density from different datasets including the global wood density database (Chave et al., 2009; Zanne et al., 2009) based on the recorded tree genus and species. Species-specific wood density was obtained for 22 different tree species. Trees whose species were unknown were assigned the average wood density of the known species.

Thereafter, the total biomass for trees with a diameter >=10cm in a sample plot was obtained by summing up individual tree AGB values. Total shrub AGB was obtained by multiplying the stem count in a plot by the estimated AGB of each stem. Total plot-level AGB was the sum of trees and

28

shrubs AGB. The final plot AGB was converted to Mg ha−1. Further, plot-level AGB was divided into *Prosopis* only and other species AGB.

3.3.2 Calculating LiDAR Metrics

To derive LiDAR metrics, LiDAR point clouds within the bounds of each field plot were extracted and analysed in two approaches. The first extracted user-defined plot level metrics of maximum height, mean height, the standard deviation of height, percentile heights (10th, 25th, 50th, 75th, 90th, and 95th), and canopy cover and density metrics (first echo cover index, all echo cover index and afci). These were calculated with a 0.3 m height threshold. 0.3 m matches the height at which stem diameters were measured while at the same time removing ground points or points hitting grass and other low-lying vegetation. **Error! Reference source not found.** shows the user-defined metrics extracted.

Table 3-7:User-defined LiDAR metrics

User-defined metric	Description
zmax	Maximum return height
zmean	Mean return height
zsd	Standard deviation of return height
zq10, zq25, zq50, zq75, zq90, zq95	10th, 25th, 50th, 75th, 90th, and 95th percentile (quantile) of the return height distribution
fci (first echo cover index)	Proportion of canopy hits above a 0.3 m height threshold. Fraction of first and single canopy echoes. (fci = ($\sum$Singlecanopy + $\sum$Firstcanopy) / $\sum$SingleAll + $\sum$FirstAll))
aci (all echo cover index)	All echo types above the height threshold 0f 0.3 m (aci = $\sum$Allcanopy / $\sum$All)
afci	All returns above the height threshold divided by the first returns

The second approach extracted standard metrics predefined by the 'stdmetrics' function in lidR package (Roussel et al., 2020, 2022) within R-studio. Standard metrics include statistical metrics like the mean, standard deviation, median, skewness, and kurtosis of the LiDAR heights and intensity; canopy height and intensity metrics computed as percentiles of the observed heights and intensities respectively; and canopy density metrics. Canopy density metrics usually divide the point clouds into 10 equal vertical intervals or slices and derive the cumulative percentage of return

heights and intensities in each interval (See more details in (Woods et al., 2008)). A total of 54 standard metrics were extracted (**Error! Reference source not found.**). Similar metrics have been used in other studies (Amara et al., 2020; Heiskanen et al., 2019).

Table 3-8: Standard metrics extracted

Standard metric	Description
zmax	Maximum return height
zmean	Mean return height
zsd	Standard deviation of return height
zskew	Skewness of return height
zkurt	Kurtosis of return height
zentropy	Measure of the randomness of the return height
pzabovezmean	Percentage of returns above zmean
pzabove2	Percentage of returns above 2m
zq5, zq10, zq15, …, zq95	5th, 10th, 15th, …, and 95th percentile (quantile) of return height distribution
zpcum1, zpcum2, zpcum3, …, zpcum9	Cumulative percentage of return height in the 1st, 2nd, 3rd,…, and 9th interval when return heights are divided into 10 equal intervals
itot	Sum of return intensities
imax	Maximum return intensity
imean	Mean return intensity
isd	standard deviation of return intensity
iskew	Skewness of return intensity
ikurt	Kurtosis of return intensity
ipground	Percentage of return intensity from ground points
ipcumzq10	Percentage of intensity returned by points below the 10th percentile of height
ipcumzq30	Percentage of intensity returned by points below the 30th percentile of height
ipcumzq50	Percentage of intensity returned by points below the 50th percentile of height
ipcumzq70	Percentage of intensity returned by points below the 70th percentile of height
ipcumzq90	Percentage of intensity returned by points below the 90th percentile of height
p1th	Percentage of 1st returns
p2th	Percentage of 2nd returns
p3th	Percentage of 3rd returns
p4th	Percentage of 4th returns
p5th	Percentage of 5th returns
pground	Percentage of returns classified as ground points

3.3.3 Modelling Sample Plot AGB With LiDAR Metrics

Modelling was carried out in two steps. First, the 'regsubsets' function in leaps package (Miller, 2020) within R-Studio was used to fit linear regression models to user-defined and standard metrics. The function used different combinations of the extracted metrics as the predictor variables and total AGB and *Prosopis* AGB as the response variables. The function selects a small subset of predictor variables which provide good predictions of the response variable. In this study, two sets of the best combination of 1, 2, and 3 predictor variables were extracted for both total and *Prosopis* AGB. The function also returned the adjusted coefficient of determination (adjusted R^2) of the variable combinations.

Second, the 'lm' function in R was used to fit linear regression models between the predictor and response variables. The result was a summary containing key information like the residual standard error, multiple and adjusted R^2, the F-statistic and the p-value. Models containing variables with a level of significance $p<0.05$ were discarded.

3.3.4 Accuracy Assessment

Leave-one-out cross-validation (LOOCV) method was used to evaluate how well the models perform by comparing predicted with observed AGB. LOOCV is a suitable evaluation method where the dataset contains too few observations for splitting into training and testing. LOOCV works by using all but one observation for model training and then applying the resulting model to predict the AGB of the observation that was left out. The process was iterated over every observation such that each had a predicted AGB value. The following evaluation statistics between observed and predicted biomass were then computed:

$$RMSE = \sqrt{\frac{\sum_{i=1}^{n}(y_i - \hat{y}_i)}{n}}$$

(3.5)

$$R^2 = 1 - \frac{\sum_{i=1}^{n}(y_i - \hat{y}_i)^2}{\sum_{i=1}^{n}(y_i - \bar{y})^2}$$

(3.6)

$$RMSEr = \frac{RMSE}{\bar{y}} \times 100$$

31

where,

RMSE = Root mean square error

R^2 = Coefficient of determination.

RMSEr = Relative root mean square error

y = Measured AGB

ŷ = Predicted AGB

ȳ = Mean of predicted AGB

n = Number of observations

Scatter plots of predicted vs observed AGB were also made to aid in model evaluation. Models that seemed to underestimate or overestimate AGB were discarded.

3.4 Land Use and Land Cover Mapping Using Sentinel-2 Imagery

The classification was undertaken to determine *Prosopis* invaded areas and separate them from other vegetation.

3.4.1 Sentinel-2 Image Pre-Processing

Sentinel-2 satellite imagery for the period March 2021 to March 2022 was used for modelling. Specifically, 10m bands 2, 3, 4, and 8, 20m bands 5, 6, 7, 8A, 11, 12 and 60m bands 1 and 9 were applied. The bands were resampled to 10m spatial resolution. Annual metrics, namely annual median, 25th percentile (Q1), 75th percentile (Q3) and interquartile range (Q3-Q1) computed for all the bands.

Vegetation indices have been shown to enhance model performance (Immitzer et al., 2016; Ng et al., 2017). To increase the sensitivity of the imagery to different vegetation types, the annual metrics (described above) of vegetation indices Two-band Enhanced Vegetation Index (EVI2),

Green Ratio (GR), Red Edge Normalized Difference Vegetation Index (RENDVI), and Green Normalised Difference Vegetation Index (GNDVI), were retrieved:

$$EVI2 = 2.4 \times \frac{nir - red}{nir + red + 1}$$

<div align="right">(3.8)</div>

$$GR = \frac{green}{red}$$

<div align="right">(3.9)</div>

$$RENDVI = \frac{RE2 - RE1}{RE2 + RE1}$$

<div align="right">(3.10)</div>

$$GNDVI = \frac{nir - green}{nir + green}$$

<div align="right">(3.11)</div>

where nir is near-infrared band 8, red corresponds to band 4, green to band 3, RE1 to vegetation red edge band 5, and RE2 to vegetation red edge band 6.

The annual metrics were computed in Google Earth Engine and stacked into a 10m image composite.

3.4.2 LULC Classification

To predict the spatial distribution of *Prosopis* in the study area, a random forest model was fitted and validated using spatial cross-validation (Brenning, 2012). Random forest has been applied in various *Prosopis* classification problems and usually achieves good accuracies (Ahmed et al., 2021; Mbaabu et al., 2019; Meroni et al., 2017; Ng et al., 2016, 2017). In this study, the predictor set consists of Sentinel-2 bands annual metrics, vegetation indices annual metrics as well as ALS-based 10m resampled CHM, totalling 64 raster layers. The model was trained on a labelled set of 71 polygons indicating *Prosopis* and non-*Prosopis* classes.

In the study area, *Prosopis* occurred as pure; mixed with other natural trees or (and) shrub species, or mixed with agriculture. Mixed stands presented difficulties in spectrally separating *Prosopis* from the other species. Therefore, this classification only broadly classifies *Prosopis*. This study used a binary classification scheme with probability thresholds (Rembold et al., 2015). Pixels were

thus considered as not infested if their probability of belonging to class *Prosopis* was lower than the set thresholds. The threshold was fixed at 0.3. This threshold value ensured that pixels with few *Prosopis* trees—either in mixed or sparse stands—were classified as invaded.

3.4.3 Validation of the Classification

The model was validated using 10-fold cross-validation, i.e., 100 iterations of spatially segmented test datasets to reduce the effects of spatial autocorrelation and derive accuracy metrics of the model predictions (Kohavi, 2001). Given the relatively small sample size of our reference dataset, a validation approach utilizing data not used for training was not applicable as no additional ground data were available (Meroni et al., 2017). The model set-up and cross-validation were implemented in the R software package mlr3 (Lang et al., 2019).

3.5 Generation of the *Prosopis* AGB Map

A regular grid with each cell size 30×30 m corresponding to the sample plot size of 0.1 ha (1000 m^2) was generated. The grid covered the entire 58 sq. km study area. LiDAR metrics were extracted within each grid cell. Thereafter, AGB within each grid cell was computed using the selected regression model resulting in a wall-to-wall AGB map over the study area. The LULC map was used to mask out non-*Prosopis* areas to remain with a *Prosopis* AGB map.

4 RESULTS AND DISCUSSIONS

4.1 Sample Plot AGB From Allometric Models

Equation (3.1) by Muturi et al., (2012) produced unrealistically high biomass values for larger trees. The observed bias may have been caused by extrapolating beyond the maximum diameter of the allometric model sample data (Duncanson et al., 2017, 2021). While Linders et al., (2020) model seemed to have less bias than Muturi et al., (2012), it still overestimated AGB for stems with D30>18.5 cm.

Since the locally derived species-specific allometric models seemed to overestimate AGB for larger trees, general allometric models were applied. Specifically, Chave et al., (2014) equation 4 was applied for trees with D30 > 18.5cm. This is because its estimated AGB for smaller stems seemed to compare well with the results from Linders et al., (2020) model, but without overestimating the AGB of larger trees. Equation (3.4) by Conti et al., (2019) was used for estimating the AGB for shrubs of other species. In this case, Chave et al., (2014) allometric model was not applied because it was constructed from larger tree samples and may therefore be biased against smaller shrubs. Conti et al., (2019) model, on the other hand, is a shrub-specific allometric model. Figure 4-1 compares the results obtained using different allometric models.
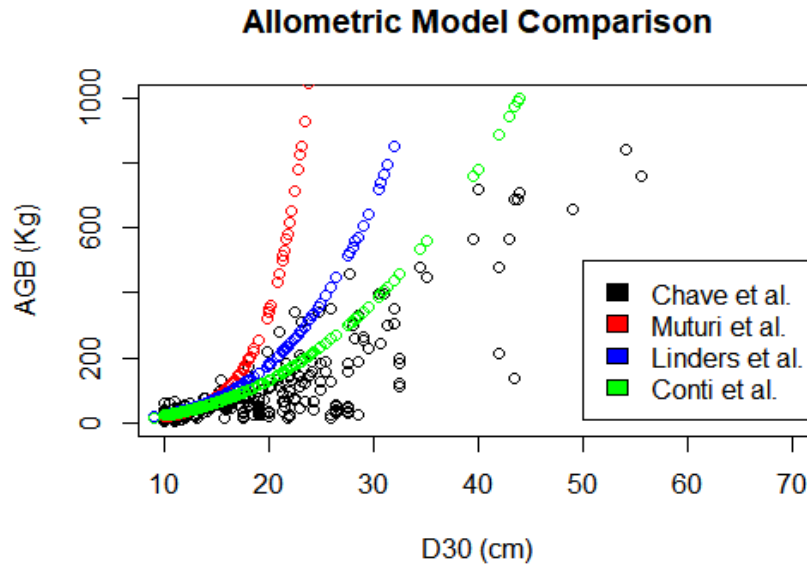
Figure 4-1: Comparison of different allometric models used in the study

The total estimated AGB was approximately 733Mg/ha with the highest plot-level estimate of 130Mg/ha. Tree-level AGB was lower than that obtained from trees with comparable diameters in Maghembe et al., (1983). This could be because the stands in Maghembe et al., (1983) were managed plantations as opposed to naturally occurring stands in this study. Other possible reasons could be differences in the *Prosopis* species (Muturi et al., 2010; Pasiecznik et al., 2001), and environmental variations. Plots with high biomass values were observed in dense *Prosopis* stands located in largely agricultural areas whereas plots with lower biomass were located in the drier areas with little agricultural activity. While field plots were selected so that the dominant species was *Prosopis*, most plots also comprised other tree and shrub species which contributed to the total AGB. The total *Prosopis* AGB was 600 Mg/ha (approximately 82% of the total AGB).

Table 4-1: Summary of estimated AGB based on field data

AGB (Mg/ha)				
	Min	**Mean**	**Max**	**Total**
Total AGB	3.396	34.893	130.299	732.753
Prosopis **AGB**	1.431	28.580	117.858	600.184

Some plots had a lower percentage (less than 50%) of *Prosopis* AGB. This may be due to a large population of shrubs of other species within the field plots.

Table 4-2: Estimated plot-level AGB based on field data

PlotID	Total AGB (Mg/ha)	*Prosopis* AGB (Mg/ha)	% *Prosopis* AGB
1	9.945	9.945	100%
2	43.780	43.780	100%
3	8.969	8.639	96%
4	19.743	19.156	97%
5	21.608	15.357	71%
7	25.301	18.166	72%
8	68.900	58.823	85%
9	3.396	3.169	93%
10	15.875	13.192	83%
10B	36.682	36.365	99%
11	130.299	117.858	90%
12	27.154	12.552	46%
13	27.083	26.607	98%
14	5.146	5.067	98%
15	30.972	11.944	39%
16	11.509	8.858	77%
17	58.775	57.316	98%
19	46.730	44.230	95%
21	99.281	69.836	70%
P1	4.890	1.431	29%
P4	36.716	17.894	49%

Besides the use of general allometric models, uncertainties in the above-computed field-plot level AGB estimates may be due to the estimation of height (H) using the H-D model, and DBH

estimation from sample measurements. These uncertainties could be reduced by using site-specific allometric equations or sampling the whole population which is beyond the scope of this study.

4.2 LiDAR Metrics

Generally, LiDAR height metrics had the strongest explanatory power on sample plot AGB. The height metric with the strongest explanatory power was zq50 which appeared in 9 out of the 12 models considered (Table 4-6). Canopy cover metrics and LiDAR intensity metrics also seemed to increase the explanatory power of height metrics on AGB.

The explanatory power of canopy cover metrics may be because an increase in canopy cover signifies more dense vegetation and thus higher AGB. For LiDAR intensity, the explanatory power may be due to the difference in intensity returned by vegetation vis-a-vis that returned by other surfaces like bare ground.

Overall, the best performing variable combination was the 3-variable combination of zq50+zq10+pground with an adjusted R^2 of 0.947 and RSE of 7.461. Using the model combination of zq50+zq10 alone yielded a lower adjusted R^2 of 0.909 and an RSE of 9.742. Therefore, pground increased model accuracy possibly because less ground returns equal more dense vegetation and thus higher AGB. The next best variable combinations were zq50+zq10+aci and zq50+ipground with an adjusted R^2 of 0.925 and 0.930, respectively. While one variable models showed good performance, the inclusion of additional variables increased their explanatory power. For both user-defined and standard metrics, it was noted that models containing zq10+zq50 generally performed better (Table 4-6).

4.3 Model Evaluation

Using LOOCV accuracy statistics, *Prosopis*-only models yielded higher RMSE with the highest being zq35+zpcum9 with RMSE of 14.9 Mg/ha (42.7% of the mean AGB). This may be because LiDAR point clouds comprise returns from all vegetation found within the field plot and not just from *Prosopis*. Nevertheless, total AGB models can be applied for modelling total AGB in the study area. A land use land cover map showing *Prosopis* invaded areas can then be used to distinguish *Prosopis* AGB.

Model performance was also analysed by plotting predicted AGB against measured AGB and checking whether they follow the 1:1 line. While one variable model variables zq50 and zq60 showed good performance and did not consistently under- or over-estimate AGB, models with more variables had increased R^2 and lower RMSE and were thus preferred.

Models zq50+zq10, zq50+zq10+aci, zq50+ipground, and zq10+zq50+pground were then used to compute AGB in the study area. In the resulting maps, the model that had an intensity variable, namely zq50+ipground, predicted AGB even on bare land, contradicting the expectation of zero AGB in such areas Furthermore, the model exhibited higher AGB than other models pointing to the fact that it was overestimating AGB. The reason for this may be because ground points also have a LiDAR intensity, and so the calculation of AGB will return a value even where there is no vegetation and AGB is expected to be zero. An alternative would be to use a LiDAR intensity threshold to remove lower values. However, this was not possible because the LiDAR intensity in the dataset was not calibrated (Kim et al., 2009). AGB map predicted using zq50+zq10+aci contained artefacts. Model variable aci is sensitive to the density of the underlying point clouds which may have caused the artefacts. For this reason, the model zq50+zq10+aci was discarded. Model variable pground showed some sensitivity to biomass with an inverse relationship where areas with fewer detected ground points had higher biomass while areas with more ground points had lower biomass. This is because detection of fewer ground points signifies denser vegetation and thus generally high biomass. However, for plots with lower biomass, there is no clear relationship between detected ground points and AGB. Further, using detected ground points may be misleading because *Prosopis* shrubs tend to be densely vegetated making it challenging for ground point detection. Such shrubs could thus be interpreted to have a higher AGB than well-spaced trees which allow detection of numerous ground points. Even though model zq50+zq10+pground exhibited the highest R^2 of 0.920 with an RMSE of 8.92Mg/ha (25.6% of the mean AGB), pground could be misleading and this model was therefore rejected.
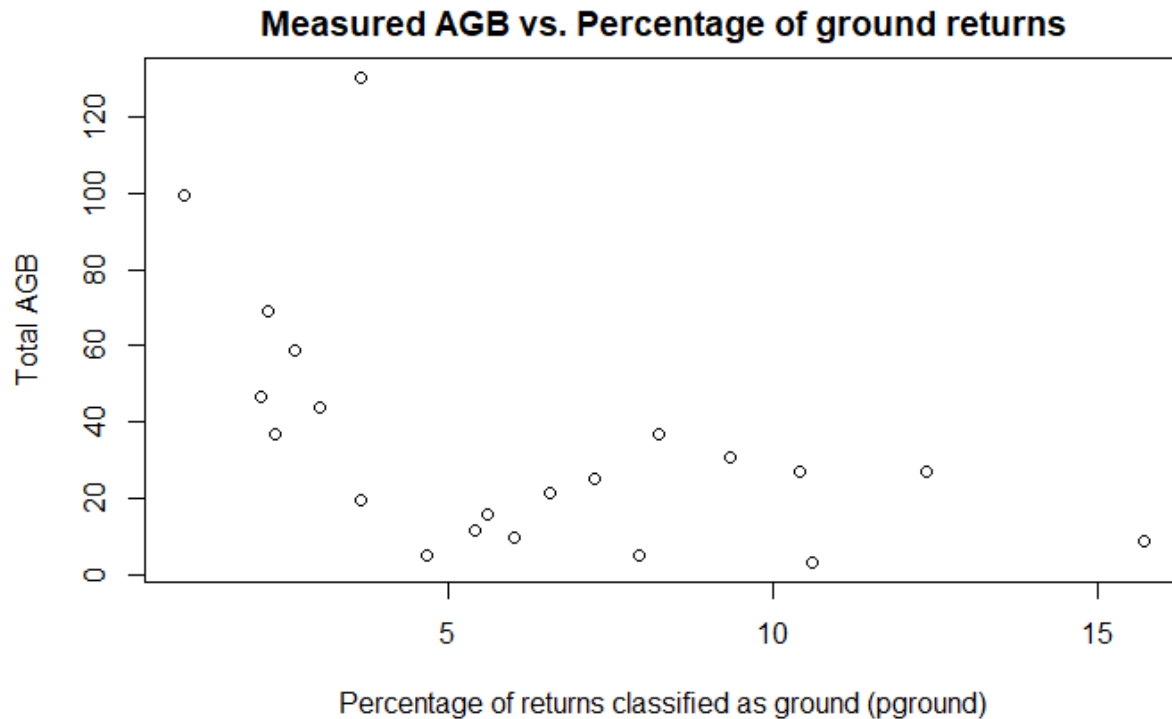
Figure 4-2: Measured AGB vs. Percentage of ground returns

Model zq50+zq10 did not contain any artefacts in the resulting AGB map and variables zq10 and zq50 show a strong relationship with AGB (Figure 4-3). While zq10 seems to be similar for plots with a low AGB, it generally increases with increasing AGB. Model zq10+zq50 was thus the best performing model and it was used for AGB estimation in the larger study area.
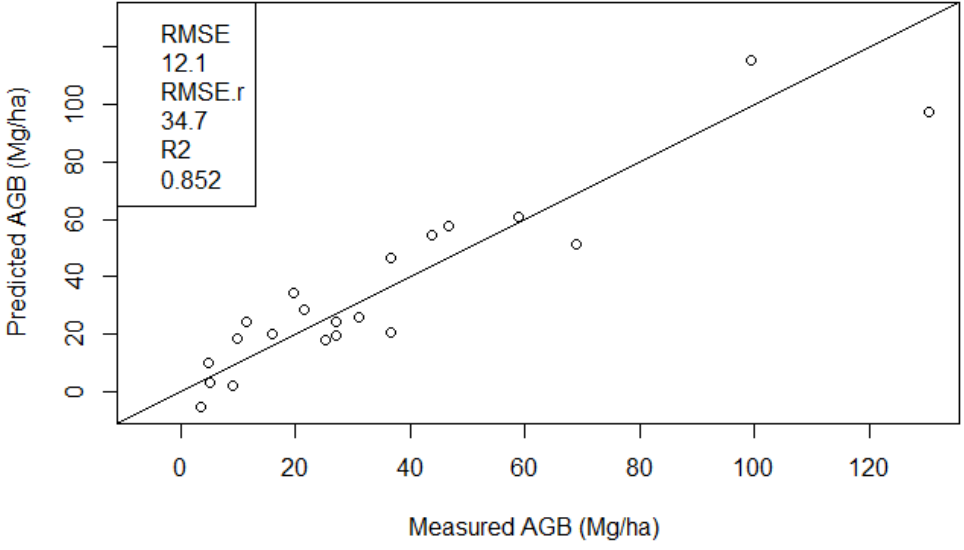
Figure 4-3: Measured AGB vs. LiDAR variables zq10 and zq50

Table 4-3: Linear regression model fit summary statistics and corresponding LOOCV evaluation results

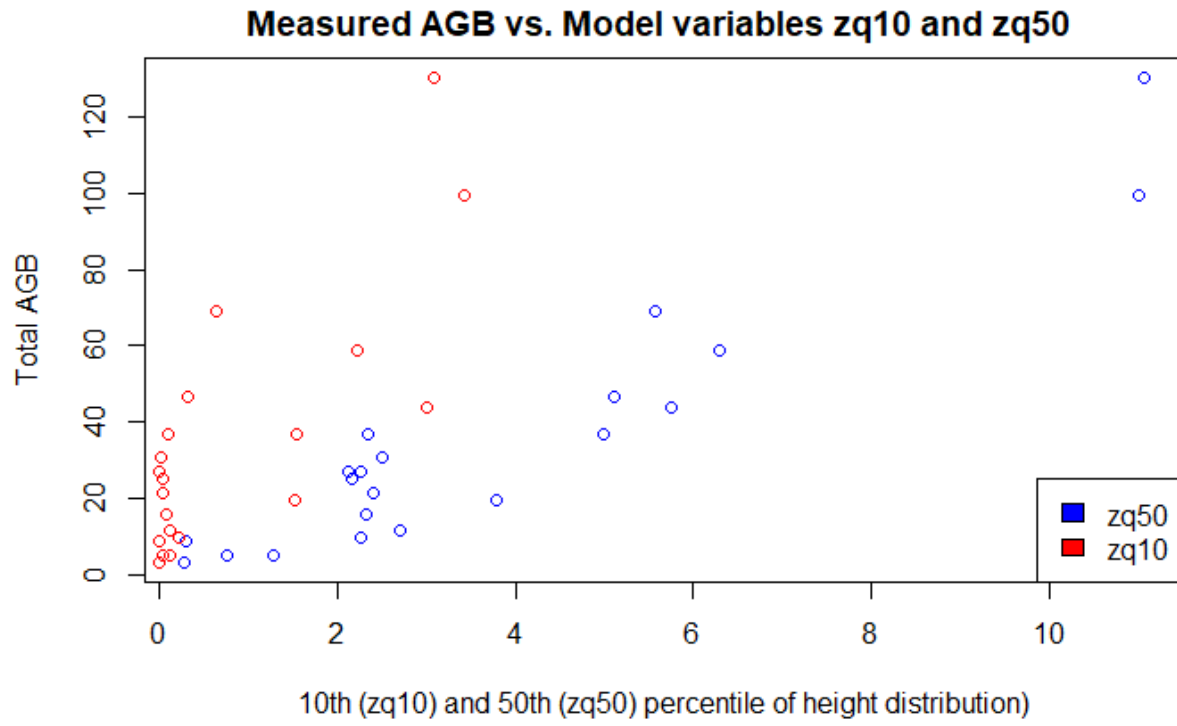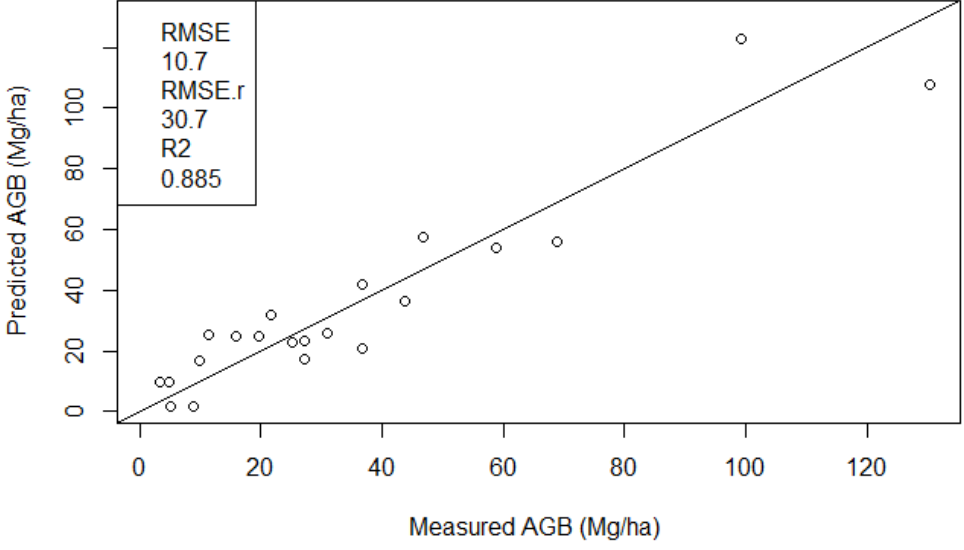|	Total AGB (Dependent Variable)							*Prosopis* AGB							
	Predictive Model	Adjusted R^2	RSE (Mg/ha)	F	P-Value	RMSE (Mg/ha)	RMSEr (%)	R^2	Models	Adjusted R^2	RSE (Mg/ha)	F	P-Value	RMSE (Mg/ha)	RMSEr (%)	R^2
User-defined metrics	zq50	0.890	10.68	163.5	<0.01	12.1	34.7	0.851	zq50	0.871	10.23	136.6	<0.01	14.7	42.1	0.829
	zq50+zq10	0.909	9.742	100.7	<0.01	11.2	32.1	0.873	zq50+aci	Models were rejected because aci and afci were found not statistically significant at p<0.05						
	zq50+zq10+aci	0.925	8.841	83.1	<0.01	10.7	30.7	0.885	zq50+aci+afci							
Standard metrics	zq60	0.893	10.55	167.9	<0.01	12.1	34.7	0.852	zq50	0.871	10.23	136.6	<0.01	14.7	42.1	0.829
	zq50+ipground	0.930	8.555	133.2	<0.01	9.84	28.2	0.902	zq35+zpcum9	0.910	8.584	101.5	<0.01	14.9	42.7	0.823
	zq10+zq50+pground	0.947	7.461	119	<0.01	8.92	25.6	0.920	zq5+zq60+ikurt	0.927	7.689	86.11	<0.01	13.8	39.5	0.871

	Total AGB	
	Model	**Scatter plot of measured vs. predicted total AGB**
User-defined metrics	**zq50**	RMSE 12.1 RMSE.r 34.7 R2 0.851 Predicted AGB (Mg/ha) vs. Measured AGB (Mg/ha)
	zq50+zq10	RMSE 11.2 RMSE.r 32.1 R2 0.873 Predicted AGB (Mg/ha) vs. Measured AGB (Mg/ha)

	zq50+ zq10+ aci	
Standard metrics	**zq60**	

zq50+ ipground	RMSE 9.84 RMSE.r 28.2 R2 0.902	
zq10+ zq50+ pground	RMSE 8.92 RMSE.r 25.6 R2 0.92	
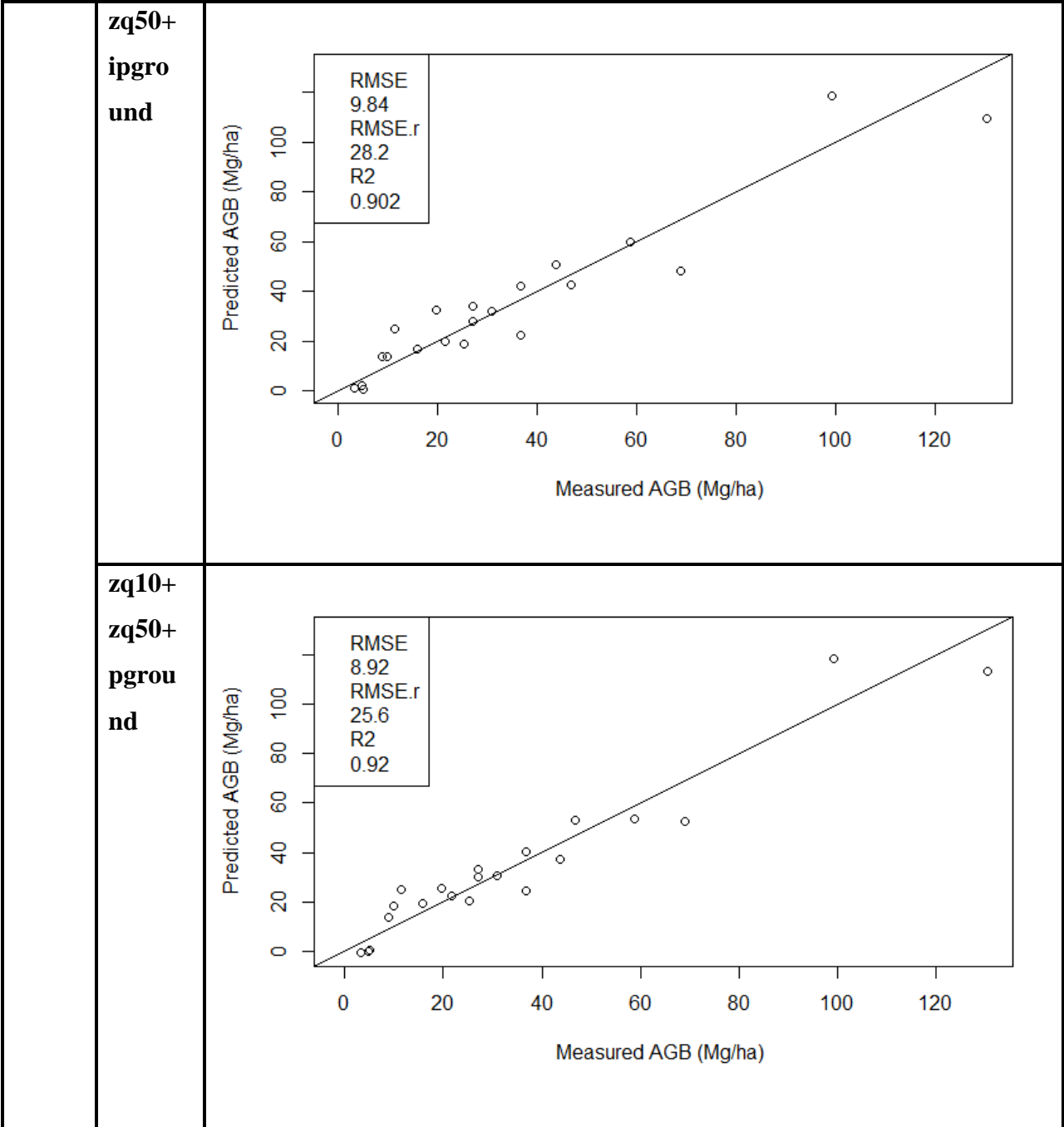
Figure 4-4: Scatter plots of measured vs, predicted AGB

4.4 Classifying *Prosopis* using Sentinel-2 Imagery

The classification results are presented in Figure 4-5. The overall accuracy achieved was approximately 86% which is comparable to that achieved by Ng et al., (2017). The probability that a pixel was assigned to class *Prosopis* was also output. Areas characterized by large, homogeneous patches of *Prosopis* invasion have high probabilities while sparsely vegetated and non-homogeneous areas have lower probabilities, similar to findings by Ng et al., (2017).

Figure 4-5: Random Forest classification results

A 0.3 threshold was applied to the classification results such that resulting in a classification map had only two classes: *Prosopis* invaded and non-invaded (Figure 4-6). Pixels below the threshold value were considered non-invaded.

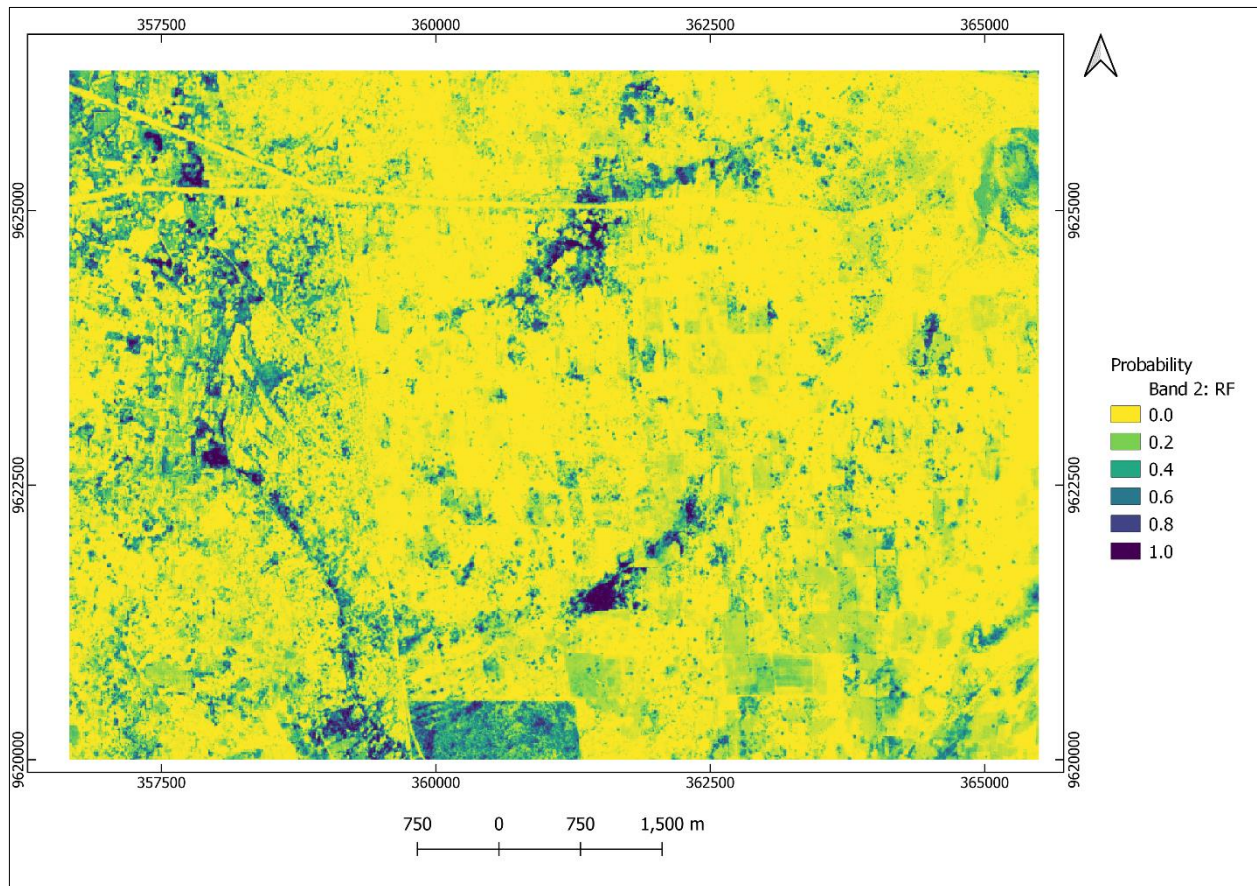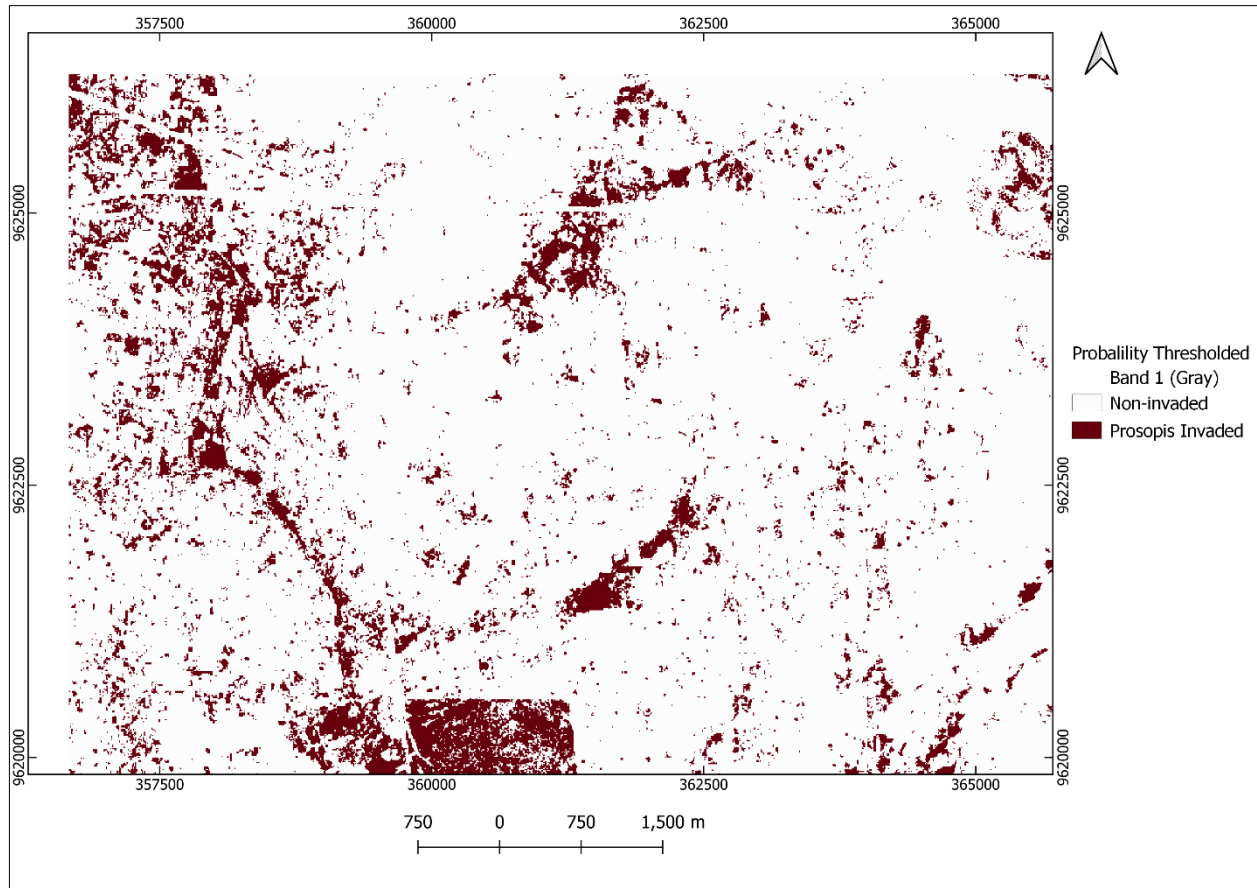*Figure 4-6: Classification results after applying the 0.3 probability threshold*

The area to the west which lies at a lower elevation and is predominantly agricultural is highly invaded. The reason for this may be that it is classified as a seasonal swamp according to Kenya 1:50000 topographic map sheet 188/3. Pasiecznik et al., (2001) observed that in dry coastal areas, *Prosopis* tended to grow well in areas with a high water table.

Prosopis has been found to initiate invasions along water sources, on abandoned farms and in urban areas (Muturi et al., 2010; Ng et al., 2016; Rembold et al., 2015). Drainage lines were created using a 30m resampled DTM (see 3.2.3.2) and overlaid on the classification map (Figure 4-7).

47
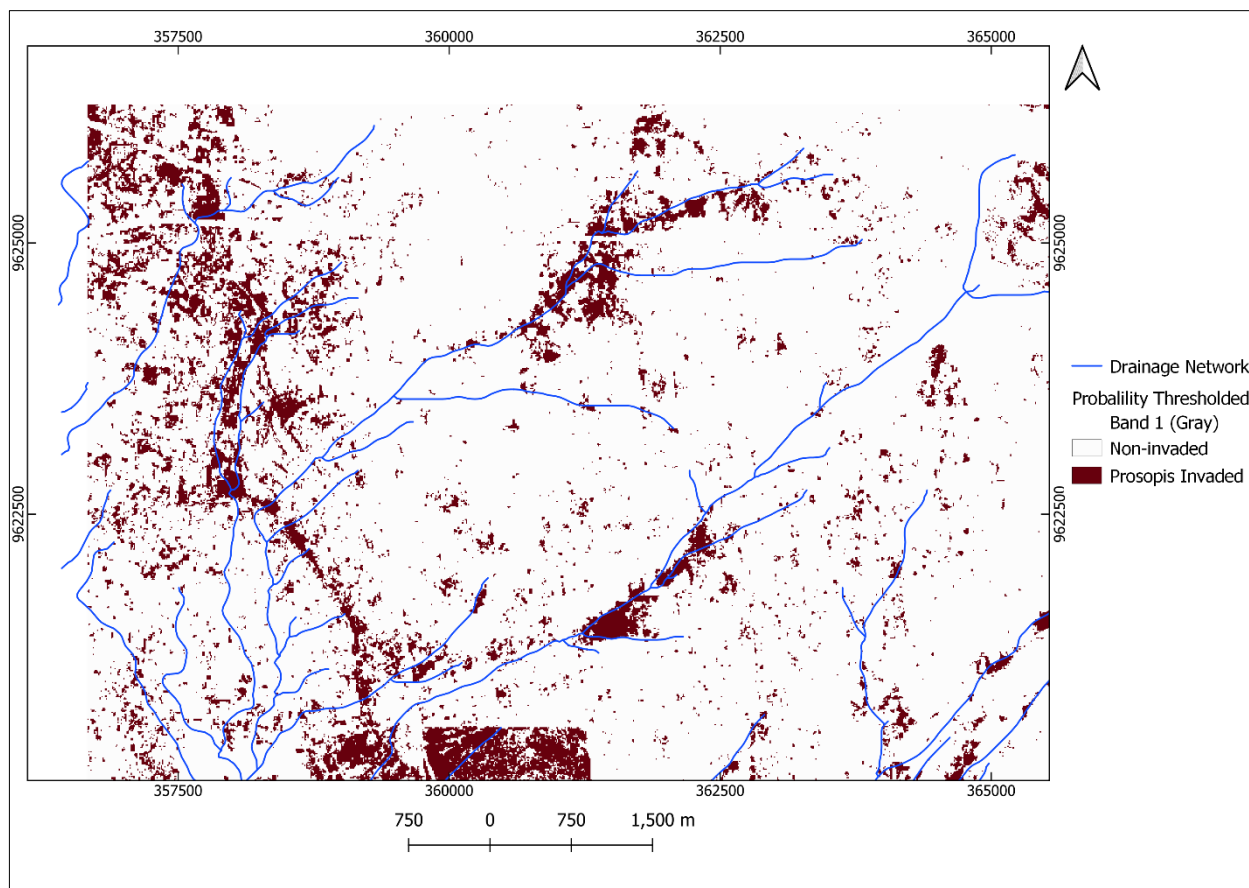
Figure 4-7: Drainage lines overlaid on classification results

Prosopis invasion was apparent along drainage lines, especially on the drier eastern side of the study area. The distribution of *Prosopis* seems to be more affected by water availability than abandoned farmlands like in Muturi et al., (2010). Similar findings have been reported by Ng et al., (2016). Rembold et al., (2015), on the other hand, mainly detected *Prosopis* in both built-up areas and water courses.

4.4.1 Variable Importance

Figure 4-8 shows the importance of variables used in the classification. The 25th percentile of Sentinel 2 band 5 (Vegetation Red Edge) was the most important for the classification. The CHM ranks 8th in importance. For the vegetation indices, the 75th percentile of GNDVI and RENDVI rank 6th and 7th respectively. Amongst the 15 most important features, three were located in the visible region (band 2,3, and 4), three in the Red Edge band (band 5), three in the coastal and

aerosol band (band 1), and three in Shortwave InfraRed region (bands 10 and 11). The remaining three spots were taken up by vegetation indices and the CHM.
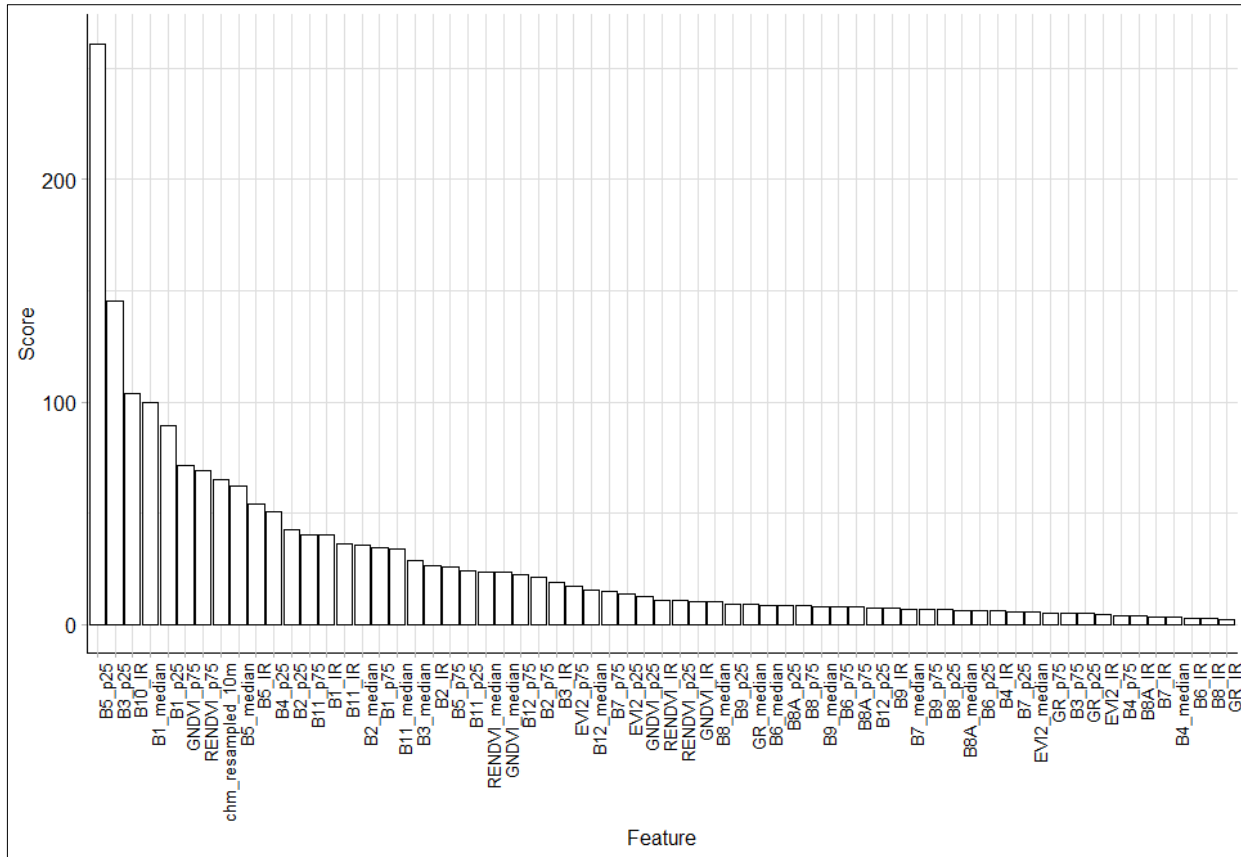
Figure 4-8: Variable importance indicating which input parameters have the greatest effect on the classification

4.5 *Prosopis* AGB Map

The best-performing model was used to produce a wall-to-wall AGB of the study area. Since the fitted model had a negative intercept, areas lacking in biomass had negative predicted values. These were set to 0. The *Prosopis* classification map (Figure 4-6) was resampled to 30m spatial resolution and used to mask out non-invaded areas to produce a *Prosopis* AGB map of the study site. AGB ranged from 0 to 313 Mg/ha.

Figure 4-9: Predicted Prosopis AGB in the study area

4.6 Discussion of the Results

4.6.1 *Prosopis* AGB from LiDAR

The results of this study revealed that LiDAR data is a practical method for estimating *Prosopis* AGB. Specifically, LiDAR height variables were found to perform best. However, it is important to note that LiDAR heights are based on the premise that taller trees generally exhibit higher biomass. But for trees which have achieved maximum heights, height distribution metrics may be a poor predictor for AGB as they may underestimate the biomass in such stands (Hansen et al., 2015).

The LiDAR point density used in this study is variable. It is likely that the uneven distribution of points has affected the variable coefficients and thus introduced errors in the wall-to-wall predictions. On the other hand, in practical applications, there is unlikely to be regular point distribution due to the overlap between adjacent stripes to minimize gaps. Thus, the differences between the sample plot and predicted values in this study may be an accurate depiction of what might be expected in practical applications.

4.6.2 *Prosopis* Classification

Both dry and wet season Sentinel 2 images were used for classification. Multiseasonal images have been found to increase classification results because they provide additional information on *Prosopis* phenology (Meroni et al., 2017). Nevertheless, dry season images have also proved equally adequate for *Prosopis* classification (Berg et al., 2013; Wakie et al., 2016) based on the assumption that compared to other vegetation species, *Prosopis* is usually the most photosynthetically active.

Prosopis was challenging to classify because, in some areas, it does not occur as a pure stand but is mixed in with other vegetation. Further, *Prosopis* presents in different forms ranging from shrubs to large trees and from dense to sparse vegetation depending on the environmental conditions. In both cases, the spectral response of a pixel will be a mix of sparse vegetation and soils or mixed species. Ultimately, the pixel value is highly influenced by the predominant land cover class leading to poorer classification results as compared to a pure *Prosopis* pixel. This may be mitigated by the use of higher spatial resolution imagery for classification (Ng et al., 2017).

Another challenge is that *Prosopis* may have similar reflectance with other vegetation making it harder to distinguish. As such, the collection of spectral signatures using field spectrometers would probably provide vital information for improving the classification since *Prosopis* is typically greener than native species during the dry season (Rembold et al., 2015). With that being said, in some cases, spectral measurements could still prove unhelpful in locations where *Prosopis* is dry and native species are green due to proximity to water resources. For example, in Meroni et al., (2017), dry *Prosopis* and healthy Acacia Spp. were found to have similar spectral reflectance.

A further limitation is that given the 10m spatial resolution of the Sentinel 2 imagery used, *Prosopis* occurring as single trees and shrubs distributed across the landscape were not detected. *Prosopis* was mainly detected in areas where it occurred in dense thickets (similar to limitations in Ayanu et al., (2015)). One more reason for the observed classification difficulties is that there were fewer reference data in areas with heterogeneous species distribution. That said, even with adequate reference data, the spatial resolution of Sentinel 2 imagery may have still been a limiting factor because the size of *Prosopis* reference polygons could be smaller compared to the resolution. Smaller reference polygons also imply fewer reference pixels for model training. The classification results are therefore better in areas with *Prosopis* as the dominant species. It is important to keep the above limitations in mind while interpreting the classification results.

Still, the maps show the potential of Sentinel 2 imagery for *Prosopis* classification even in heterogeneous areas at the stand level—as opposed to at the individual tree level (Immitzer et al., 2016). The classification is thus suitable for determining areas with established *Prosopis* invasions versus areas with sparse or mixed invasions, or those in the initial stages of invasion. The classification map may be utilized to identify areas that should be prioritized for *Prosopis* control and management as well as monitoring.

The feature importance shows the value of Sentinel 2 red-edge and shortwave infrared bands for vegetation species classification (Immitzer et al., 2016). The red edge part of the electromagnetic spectrum is important for the detection of vegetation chlorophyll content (Ku & Popescu, 2019), Given that *Prosopis* is evergreen throughout the year, the importance of band 5 is not surprising. Unlike in Ng et al., (2017), the Green Ratio index (GR) was not among the most important features for *Prosopis* identification.

Prosopis was mainly detected along water courses and low-lying regions where water from higher elevations drains. These results confirm that *Prosopis* competes with native vegetation for water resources. Further, that watercourses are a major transportation route for *Prosopis* seeds (Pasiecznik et al., 2001) likely explains the high presence of *Prosopis* in the agricultural area on the western side of the study area.

5   CONCLUSIONS, RECOMMENDATIONS AND AREAS FOR FURTHER RESEARCH

5.1 Conclusions

In this study, LiDAR variables were extracted and used to predict the AGB of naturally occurring *Prosopis* in the study area. Upon accuracy assessment, the best results were achieved by using a model with height distribution metrics namely the 10th percentile (zq10) and 50th percentile (zq50) of height. On accuracy assessment, the resulting model had an R^2 of 0.873 and RMSE of 11.3Mg/ha (32.1% of the mean). This model was used to generate a *Prosopis* AGB map of the study area. These results demonstrate the effectiveness of LiDAR for AGB mapping of *Prosopis*.

5.2 Recommendations

The density of LiDAR points used in this study varied across the landscape which may have affected the LiDAR variables selected. Using LiDAR data with even distribution of point clouds should be considered in the future. The accuracy assessment could be improved by evaluating the level of overfitting of the sample data by computing the sum of squares ratio (SSR). The number of field plots sampled in this study is fairly small. The study could further be improved by incorporating more sample plots to cover areas with varying terrain, and vegetation types hence improving the model. Further, the collection of more sample plots could avail additional data for LiDAR model evaluation improving the reliability of the resulting AGB map.

5.3 Areas for Further Research

Allometric equations are a major source of uncertainty in biomass estimation (Zolkos et al., 2013). In this study, a lack of *Prosopis* allometric models that capture large *Prosopis* trees such as those found in Taveta was a limitation, pointing out a potential area for further study.

Combining LiDAR data with optical remote sensing data has been shown to increase the accuracy of AGB predictive models (Zolkos et al., 2013). The contribution of optical remote sensing when integrated with LiDAR data for *Prosopis* AGB is an area for further investigation.

REFERENCES

Adoyo, B., Choge, S. K., Eckert, S., Ehrensperger, A., Eschen, R., Kilawe, C. J., Kiteme, B., & Schaffner, U. (2021). *Integrating the control of invasive trees in land use and management plans*. The Woody Weeds Project. Practice Brief. https://woodyweeds.org/wp-content/uploads/2021/10/WoodyWeeds-Practice-Brief-Integration.pdf

Ahmed, N., Atzberger, C., & Zewdie, W. (2021). Species Distribution Modelling performance and its implication for Sentinel-2-based prediction of invasive Prosopis juliflora in lower Awash River basin, Ethiopia. *Ecological Processes*, *10*(1), 18. https://doi.org/10.1186/s13717-021-00285-6

Amara, E., Adhikari, H., Heiskanen, J., Siljander, M., Munyao, M., Omondi, P., & Pellikka, P. (2020). Aboveground Biomass Distribution in a Multi-Use Savannah Landscape in Southeastern Kenya: Impact of Land Use and Fences. *Land*, *9*(10), 381. https://doi.org/10.3390/land9100381

Andersson, S. (2005, February 3). *Spread of the introduced tree species Prosopis juliflora (Sw.) DC in the Lake Baringo area, Kenya* [Other]. SLU, Dept. of Forest Ecology and Management. https://stud.epsilon.slu.se/10961/

Ayanu, Y., Jentsch, A., Müller-Mahn, D., Rettberg, S., Romankiewicz, C., & Koellner, T. (2015). Ecosystem engineer unleashed: Prosopis juliflora threatening ecosystem services? *Regional Environmental Change*, *15*(1), 155–167. https://doi.org/10.1007/s10113-014-0616-x

Berg, E. V. den, Kotze, I., & Beukes, H. (2013). Detection, Quantification and Monitoring of Prosopis in the Northern Cape Province of South Africa using Remote Sensing and GIS. *South African Journal of Geomatics*, *2*(2), 68–81. https://doi.org/10.4314/sajg.v2i2

Brenning, A. (2012). Spatial cross-validation and bootstrap for the assessment of prediction rules in remote sensing: The R package sperrorest. *2012 IEEE International Geoscience and Remote Sensing Symposium*, 5372–5375. https://doi.org/10.1109/IGARSS.2012.6352393

Chave, J., Condit, R., Aguilar, S., Hernandez, A., Lao, S., & Perez, R. (2004). Error propagation and scaling for tropical forest biomass estimates. *Philosophical Transactions of the Royal Society B: Biological Sciences*, *359*(1443), 409–420.

Chave, J., Coomes, D., Jansen, S., Lewis, S. L., Swenson, N. G., & Zanne, A. E. (2009). Towards a worldwide wood economics spectrum. *Ecology Letters*, *12*(4), 351–366. https://doi.org/10.1111/j.1461-0248.2009.01285.x

Chave, J., Réjou-Méchain, M., Búrquez, A., Chidumayo, E., Colgan, M. S., Delitti, W. B. C., Duque, A., Eid, T., Fearnside, P. M., Goodman, R. C., Henry, M., Martínez-Yrízar, A., Mugasha, W. A., Muller-Landau, H. C., Mencuccini, M., Nelson, B. W., Ngomanda, A., Nogueira, E. M., Ortiz-Malavassi, E., … Vieilledent, G. (2014). Improved allometric models to estimate the aboveground biomass of tropical trees. *Global Change Biology*, *20*(10), 3177–3190. https://doi.org/10.1111/gcb.12629

Chen, Q., Vaglio Laurin, G., Battles, J. J., & Saah, D. (2012). Integration of airborne lidar and vegetation types derived from aerial photography for mapping aboveground live biomass. *Remote Sensing of Environment*, *121*, 108–117. https://doi.org/10.1016/j.rse.2012.01.021

Chidumayo, E. N., & Gumbo, D. J. (2010). *The dry forests and woodlands of Africa: Managing for products and services*. Earthscan. https://cgspace.cgiar.org/handle/10568/20499

Choge, S., & Pasiecznik, N. (2005). *The challenges of eradicating Prosopis in Kenya.* https://www.gov.uk/research-for-development-outputs/the-challenges-of-eradicating-prosopis-in-kenya

Conti, G., Gorné, L. D., Zeballos, S. R., Lipoma, M. L., Gatica, G., Kowaljow, E., Whitworth-Hulse, J. I., Cuchietti, A., Poca, M., Pestoni, S., & Fernandes, P. M. (2019). Developing allometric models to predict the individual aboveground biomass of shrubs worldwide. *Global Ecology and Biogeography*, *28*(7), 961–975. https://doi.org/10.1111/geb.12907

Duncanson, L., Armston, J., Disney, M., Avitabile, V., Barbier, N., Calders, K., Carter, S., Chave, J., Herold, M., MacBean, N., McRoberts, R., Minor, D., Paul, K., Réjou-Méchain, M., Roxburgh, S., Williams, M., Albinet, C., Baker, T., Bartholomeus, H., … Margolis, H. (2021). *Aboveground Woody Biomass Product Validation: Good Practices Protocol*. http://repository.si.edu/xmlui/handle/10088/110741

Duncanson, L., Huang, W., Johnson, K., Swatantran, A., McRoberts, R. E., & Dubayah, R. (2017). Implications of allometric model selection for county-level biomass mapping. *Carbon Balance and Management*, *12*(1), 18. https://doi.org/10.1186/s13021-017-0086-9

Dzikiti, S., Schachtschneider, K., Naiken, V., Gush, M., Moses, G., & Le Maitre, D. C. (2013). Water relations and the effects of clearing invasive Prosopis trees on groundwater in an

arid environment in the Northern Cape, South Africa. *Journal of Arid Environments*, *90*, 103–113. https://doi.org/10.1016/j.jaridenv.2012.10.015

Economic and Social Impacts | National Invasive Species Information Center. (n.d.). Retrieved 14 March 2022, from https://www.invasivespeciesinfo.gov/subject/economic-and-social-impacts

Esbenshade, H. W., & Grainger, A. (1980). The Bamburi Reclamation Project. *International Tree Crops Journal*, *1*(2–3), 199–202. https://doi.org/10.1080/01435698.1980.9752729

Garner, R. (2015, April 1). *Landsat Overview* [Text]. NASA. http://www.nasa.gov/mission_pages/landsat/overview/index.html

Hansen, E. H., Gobakken, T., Bollandsås, O. M., Zahabu, E., & Næsset, E. (2015). Modeling Aboveground Biomass in Dense Tropical Submontane Rainforest Using Airborne Laser Scanner Data. *Remote Sensing*, *7*(1), 788–807. https://doi.org/10.3390/rs70100788

Haregeweyn, N., Tsunekawa, A., Tsubo, M., Meshesha, D., & Melkie, A. (2013). Analysis of the invasion rate, impacts and control measures of Prosopis juliflora: A case study of Amibara District, Eastern Ethiopia. *Environmental Monitoring and Assessment*, *185*(9), 7527–7542. https://doi.org/10.1007/s10661-013-3117-3

Heiskanen, J., Adhikari, H., Piiroinen, R., Packalen, P., & Pellikka, P. K. E. (2019). Do airborne laser scanning biomass prediction models benefit from Landsat time series, hyperspectral data or forest classification in tropical mosaic landscapes? *International Journal of Applied Earth Observation and Geoinformation*, *81*, 176–185. https://doi.org/10.1016/j.jag.2019.05.017

Hoshino, B., Karamalla, A., Abd Elbasit, M., Manayeva, K., Yoda, K., Suliman, M., Ibrahim, M. E., Nawata, H., & Yasuda, H. (2012). Evaluating the Invasion Strategic of Mesquite (Prosopis juliflora) in Eastern Sudan Using Remotely Sensed Technique. *Journal of Arid Land Studies*, *22*, 1–4.

Huang, C., & Asner, G. P. (2009). Applications of Remote Sensing to Alien Invasive Plant Studies. *Sensors*, *9*(6), 4869–4889. https://doi.org/10.3390/s90604869

Iannone, B., Carnevale, S., Main, M., Hill, J., McConnell, J., Johnson, S., Enloe, S., Andreu, M., Bell, E., Cuda, J., & Baker, S. (2021). Invasive Species Terminology: Standardizing for Stakeholder Education. *The Journal of Extension*, *58*(3). https://tigerprints.clemson.edu/joe/vol58/iss3/27

Immitzer, M., Vuolo, F., & Atzberger, C. (2016). First Experience with Sentinel-2 Data for Crop and Tree Species Classifications in Central Europe. *Remote Sensing*, *8*(3), 166. https://doi.org/10.3390/rs8030166

International Organization for Standardization (ISO). (2016). *ISO/TS 19159-2:2016(en), Geographic information—Calibration and validation of remote sensing imagery sensors and data—Part 2: Lidar*. https://www.iso.org/obp/ui#iso:std:iso:ts:19159:-2:ed-1:v1:en:term:4.33

IUCN (International Union for the Conservation of Nature). (2010, May 20). *Are protected areas in Africa harbouring invasive species?* IUCN. https://www.iucn.org/content/are-protected-areas-africa-harbouring-invasive-species

KEFRI. (2020). *Unlocking the Economic Potentials of Prosopis in the Face of Changing Climate: Proceedings of the 2nd National Prosopis Management Workshop, held at Soi Safari Lodge, Lake Baringo, 18th—23rd May 2015, KEFRI Muguga, Kenya*. KEFRI. http://197.248.75.118:8282/jspui/bitstream/123456789/1014/1/UNLOCKING%20THE%20ECONOMIC%20POTENTIALS%20OF%20PROSOPIS%20IN%20THE%20FACE%20OF%20CHANGING%20CLIMATE.pdf

Kenya Law: CXI No. 2—9th January 2009. (2009, January 9). http://kenyalaw.org/kl/index.php?id=3194

Kohavi, R. (2001). *A Study of Cross-Validation and Bootstrap for Accuracy Estimation and Model Selection*. *14*.

Ku, N.-W., & Popescu, S. C. (2019). A comparison of multiple methods for mapping local-scale mesquite tree aboveground biomass with remotely sensed data. *Biomass and Bioenergy*, *122*, 270–279. https://doi.org/10.1016/j.biombioe.2019.01.045

Kyuma, R., Kinama, J., Wahome, R., Wasonga, V., & Pierre, H. M. J. (2018). Estimating above-ground biomass and carbon stocks of Prosopis juliflora using allometric equations in drylands of Magadi, Kenya. *International Journal of Agronomy and Agricultural Research (IJAAR)*, *13*(4), 92–103.

Lang, M., Binder, M., Richter, J., Schratz, P., Pfisterer, F., Coors, S., Au, Q., Casalicchio, G., Kotthoff, L., & Bischl, B. (2019). mlr3: A modern object-oriented machine learning framework in R. *Journal of Open Source Software*, *4*(44), 1903. https://doi.org/10.21105/joss.01903

Laxen, J. (2007). *Is prosopis a curse or a blessing?: An ecological-economic analysis of an invasive alien tree species in Sudan* [Doctoral Thesis]. University of Helsinki, Viikki Tropical Resources Institute (VITRI).

Linders, T. E., Bekele, K., Schaffner, U., Allan, E., Alamirew, T., Choge, S. K., Eckert, S., Haji, J., Muturi, G., Mbaabu, P. R., Shiferaw, H., & Eschen, R. (2020). The impact of invasive species on social-ecological systems: Relating supply and use of selected provisioning ecosystem services. *Ecosystem Services*, *41*, 101055. https://doi.org/10.1016/j.ecoser.2019.101055

Maghembe, J. A., Kariuki, E. M., & Haller, R. D. (1983). Biomass and nutrient accumulation in young Prosopis juliflora at Mombasa, Kenya. *Agroforestry Systems*, *1*(4), 313–321. https://doi.org/10.1007/BF00155938

Maundu, P., Kibet, S., Morimoto, Y., Imbumi, M., & Adeka, R. (2009). Impact of Prosopis juliflora on Kenya's semi-arid and arid ecosystems and local livelihoods. *Biodiversity*, *10*(2–3), 33–50. https://doi.org/10.1080/14888386.2009.9712842

Mbaabu, P. R., Ng, W.-T., Schaffner, U., Gichaba, M., Olago, D., Choge, S., Oriaso, S., & Eckert, S. (2019). Spatial Evolution of Prosopis Invasion and its Effects on LULC and Livelihoods in Baringo, Kenya. *Remote Sensing*, *11*(10), 1217. https://doi.org/10.3390/rs11101217

Mbaabu, P. R., Olago, D., Gichaba, M., Eckert, S., Eschen, R., Oriaso, S., Choge, S. K., Linders, T. E. W., & Schaffner, U. (2020). Restoration of degraded grasslands, but not invasion by Prosopis juliflora, avoids trade-offs between climate change mitigation and other ecosystem services. *Scientific Reports*, *10*(1), 20391. https://doi.org/10.1038/s41598-020-77126-7

Meroni, M., Ng, W.-T., Rembold, F., Leonardi, U., Atzberger, C., Gadain, H., & Shaiye, M. (2017). Mapping Prosopis juliflora in West Somaliland with Landsat 8 Satellite Imagery and Ground Information. *Land Degradation & Development*, *28*(2), 494–506. https://doi.org/10.1002/ldr.2611

Miller, T. L. based on F. code by A. (2020). *leaps: Regression Subset Selection* (3.1). https://CRAN.R-project.org/package=leaps

Ministry of Energy & Clean Cooking Association of Kenya. (2019). *KENYA HOUSEHOLD COOKING SECTOR STUDY Assessment of the Supply and Demand of Cooking Solutions*

at the Household Level. https://eedadvisory.com/wp-content/uploads/2020/09/MoE-2019-Kenya-Cooking-Sector-Study-compressed.pdf

Muturi, G. M., Kariuki, J. G., Poorter, L., & Mohren, G. M. J. (2012). Allometric equations for estimating biomass in naturally established Prosopis stands in Kenya. *Journal of Horticulture and Forestry*, *4*(4), 68–77. https://doi.org/10.5897/JHF11.066

Muturi, G. M., Machua, J. M., Mohren, G. M. J., Poorter, L., Gicheru, J. M., & Maina, L. W. (2012). Genetic diversity of Kenyan Prosopis populations based on random amplified polymorphic DNA markers. *African Journal of Biotechnology*, *11*(87), 15291–15302. https://doi.org/10.4314/ajb.v11i87

Muturi, G. M., Mohren, G. M. J., & Kimani, J. N. (2010). Prediction of Prosopis species invasion in Kenya using geographical information system techniques. *African Journal of Ecology*, *48*(3), 628–636. https://doi.org/10.1111/j.1365-2028.2009.01157.x

Næsset, E. (2002). Predicting forest stand characteristics with airborne scanning laser using a practical two-stage procedure and field data. *Remote Sensing of Environment*, *80*(1), 88–99. https://doi.org/10.1016/S0034-4257(01)00290-5

NEMA. (n.d.). *TAITA TAVETA DISTRICT ENVIRONMENT ACTION PLAN 2009-2013*. Retrieved 25 April 2022, from https://www.nema.go.ke/images/Docs/Awarness%20Materials/NEAPS/taita_taveta.pdf

Ng, W.-T., Immitzer, M., Floriansitz, M., Vuolo, F., Luminari, L., Adede, C., Wahome, R., & Atzberger, C. (2016). Mapping Prosopis spp. Within the Tarach water basin, Turkana, Kenya using Sentinel-2 imagery. *Remote Sensing for Agriculture, Ecosystems, and Hydrology XVIII*, *9998*, 161–173. https://doi.org/10.1117/12.2241279

Ng, W.-T., Rima, P., Einzmann, K., Immitzer, M., Atzberger, C., & Eckert, S. (2017). Assessing the Potential of Sentinel-2 and Pléiades Data for the Detection of Prosopis and Vachellia spp. In Kenya. *Remote Sensing*, *9*(1), 74. https://doi.org/10.3390/rs9010074

Obiri, J. F. (2011). Invasive plant species and their disaster-effects in dry tropical forests and rangelands of Kenya and Tanzania. *JAMBA : Journal of Disaster Risk Studies*, *3*(2), 417–428.

Pasiecznik, N. (2018). *Information on measures and related costs in relation to species considered for inclusion on the Union list: Prosopis juliflora. Technical note prepared by IUCN for*

the *European Commission*. https://circabc.europa.eu/sd/a/30b8a728-06b9-401f-a940-9531636e8fe9/TSSR%20Task%202018%20Prosopis%20juliflora.pdf

Pasiecznik, N., Choge, S., Fre, Z., Tsegay, B., & Parra, F. (2015, November 1). *The Great Green Forest is here and expanding all on its own: A call for action*.

Pasiecznik, N., Choge, S. K., Muthike, G., Chesang, S., Fehr, C., Bakewell-Stone, P., Wright, J., & Harris, P. (2006). *Putting Knowledge on Prosopis into Use in Kenya. Pioneering Advances in 2006.* KEFRI, Nairobi, Kenya and HDRA, Coventry, UK.

Pasiecznik, N., Choge, S. K., Rosenfeld, A. B., & Harris, P. (2008, January 1). *Underutilised Crops for Famine and Poverty Alleviation: A Case Study on the Potential of the Multipurpose Prosopis Tree*.

Pasiecznik, N., Harris, P., Harsh, L., Cruz, G., Tewari, J., Cadoret, K., & Maldonado, L. (2001). *The Prosopis juliflora -Prosopis pallida Complex: A Monograph*. HDRA, Coventry, UK. https://www.gardenorganic.org.uk/sites/www.gardenorganic.org.uk/files/resources/international/ProsopisMonographComplete.pdf

Petition 466 of 2006—Kenya Law. (2007). http://kenyalaw.org/caselaw/cases/view/41547/

Phua, M.-H., Johari, S. A., Wong, O. C., Ioki, K., Mahali, M., Nilus, R., Coomes, D. A., Maycock, C. R., & Hashim, M. (2017). Synergistic use of Landsat 8 OLI image and airborne LiDAR data for above-ground biomass estimation in tropical lowland rainforests. *Forest Ecology and Management*, *406*, 163–171. https://doi.org/10.1016/j.foreco.2017.10.007

Ratnayake, R. M. C. S. (2014, November 27). *Why plant species become invasive?*

Réjou-Méchain, M., Tanguy, A., Piponiot, C., Chave, J., & Hérault, B. (2017). biomass: An r package for estimating above-ground biomass and its uncertainty in tropical forests. *Methods in Ecology and Evolution*, *8*(9), 1163–1167. https://doi.org/10.1111/2041-210X.12753

Réjou-Méchain, M., Tymen, B., Blanc, L., Fauset, S., Feldpausch, T. R., Monteagudo, A., Phillips, O. L., Richard, H., & Chave, J. (2015). Using repeated small-footprint LiDAR acquisitions to infer spatial and temporal variations of a high-biomass Neotropical forest. *Remote Sensing of Environment*, *169*, 93–101. https://doi.org/10.1016/j.rse.2015.08.001

Rembold, F., Leonardi, U., Ng, W.-T., Gadain, H., Meroni, M., & Atzberger, C. (2015). Mapping areas invaded by Prosopis juliflora in Somaliland on Landsat 8 imagery. *Remote Sensing*

for Agriculture, Ecosystems, and Hydrology XVII, *9637*, 295–306. https://doi.org/10.1117/12.2193133

Roussel, J.-R., Auty, D., Coops, N. C., Tompalski, P., Goodbody, T. R. H., Meador, A. S., Bourdon, J.-F., de Boissieu, F., & Achim, A. (2020). lidR: An R package for analysis of Airborne Laser Scanning (ALS) data. *Remote Sensing of Environment*, *251*, 112061. https://doi.org/10.1016/j.rse.2020.112061

Roussel, J.-R., documentation), D. A. (Reviews the, features), F. D. B. (Fixed bugs and improved catalog, segment_snags()), A. S. M. (Implemented wing2015() for, track_sensor()), B. J.-F. (Contributed to R. for, track_sensor()), G. D. (Implemented G. for, management), L. S. (Contributed to parallelization, & code), S. A. (Author of the C. concaveman. (2022). *lidR: Airborne LiDAR Data Manipulation and Visualization for Forestry Applications* (4.0.1). https://CRAN.R-project.org/package=lidR

Roxburgh, S. H., Paul, K. I., Clifford, D., England, J. R., & Raison, R. J. (2015). Guidelines for constructing allometric models for the prediction of woody biomass: How many individuals to harvest? *Ecosphere*, *6*(3), art38. https://doi.org/10.1890/ES14-00251.1

Sentinel-2—Missions—Sentinel Online—Sentinel Online. (n.d.). Retrieved 15 August 2022, from https://sentinel.esa.int/web/sentinel/missions/sentinel-2

Shackleton, R. T., Le Maitre, D. C., Pasiecznik, N. M., & Richardson, D. M. (2014). Prosopis: A global assessment of the biogeography, benefits, impacts and management of one of the world's worst woody invasive plant taxa. *AoB PLANTS*, *6*, plu027. https://doi.org/10.1093/aobpla/plu027

Tilahun, S. L., & Asfaw, A. (2012). Modeling the expansion of Prosopis juliflora and determining its optimum utilization rate to control the invasion in Afar Regional State of Ethiopia. *International Journal of Applied Mathematical Research*, *1*(4), 726–743. https://doi.org/10.14419/ijamr.v1i4.200

Tuwei, P., Odera, E. C., Kiprop, J., & Wanjiku, J. (2019). Management of Prosopis Juliflora Invasion in Baringo County, Kenya through Utilization. *Journal of Economics and Sustainable Development*, *10*(10), 78.

Valbuena, R., Hernando, A., Manzanera, J. A., Görgens, E. B., Almeida, D. R. A., Mauro, F., García-Abril, A., & Coomes, D. A. (2017). Enhancing of accuracy assessment for forest above-ground biomass estimates obtained from remote sensing via hypothesis testing and

overfitting evaluation. *Ecological Modelling*, *366*, 15–26. https://doi.org/10.1016/j.ecolmodel.2017.10.009

Wakie, T. T., Hoag, D., Evangelista, P. H., Luizza, M., & Laituri, M. (2016). Is control through utilization a cost effective Prosopis juliflora management strategy? *Journal of Environmental Management*, *168*, 74–86. https://doi.org/10.1016/j.jenvman.2015.11.054

Walter, K. (2011). *Prosopis, an Alien among the Sacred Trees of South India* [Doctoral Thesis]. University of Helsinki, Viikki Tropical Resources Institute (VITRI).

Wilgen, B. W. van, Forsyth, G. G., Le Maitre, D. C., Wannenburgh, A., Kotzé, J. D. F., van den Berg, E., & Henderson, L. (2012). An assessment of the effectiveness of a large, national-scale invasive alien plant control strategy in South Africa. *Biological Conservation*, *148*(1), 28–38. https://doi.org/10.1016/j.biocon.2011.12.035

Wise, R. M., van Wilgen, B. W., & Le Maitre, D. C. (2012). Costs, benefits and management options for an invasive alien tree species: The case of mesquite in the Northern Cape, South Africa. *Journal of Arid Environments*, *84*, 80–90. https://doi.org/10.1016/j.jaridenv.2012.03.001

Witt, A. B. R. (2010). Biofuels and invasive species from an African perspective – a review. *GCB Bioenergy*, *2*(6), 321–329. https://doi.org/10.1111/j.1757-1707.2010.01063.x

Witt, A., & Luke, Q. (Eds.). (2017). *Guide to the naturalized and invasive plants of Eastern Africa*. CABI. https://doi.org/10.1079/9781786392145.0000

Woods, M., Lim, K., & Treitz, P. (2008). Predicting forest stand variables from LiDAR data in the Great Lakes – St. Lawrence forest of Ontario. *The Forestry Chronicle*, *84*(6), 827–839. https://doi.org/10.5558/tfc84827-6

World Agroforestry. (n.d.). *Agrofostree Species profile*. Retrieved 30 June 2022, from https://apps.worldagroforestry.org/treedb2/speciesprofile.php?Spid=1354

Wulder, M. A., Hilker, T., White, J. C., Coops, N. C., Masek, J. G., Pflugmacher, D., & Crevier, Y. (2015). Virtual constellations for global terrestrial monitoring. *Remote Sensing of Environment*, *170*, 62–76. https://doi.org/10.1016/j.rse.2015.09.001

Zachariades, C., Hoffmann, J. H., & Roberts, A. P. (2011). Biological Control of Mesquite (Prosopis Species) (Fabaceae) in South Africa. *African Entomology*, *19*(2), 402–415. https://doi.org/10.4001/003.019.0230

Zanne, A. E., Lopez-Gonzalez, G., Coomes, D. A., Ilic, J., Jansen, S., Lewis, S. L., Miller, R. B., Swenson, N. G., Wiemann, M. C., & Chave, J. (2009). *Data from: Towards a worldwide wood economics spectrum* (Version 5, p. 2047488 bytes) [Data set]. Dryad. https://doi.org/10.5061/DRYAD.234

Zhao, Y., Liu, X., Wang, Y., Zheng, Z., Zheng, S., Zhao, D., & Bai, Y. (2021). UAV-based individual shrub aboveground biomass estimation calibrated against terrestrial LiDAR in a shrub-encroached grassland. *International Journal of Applied Earth Observation and Geoinformation*, *101*, 102358. https://doi.org/10.1016/j.jag.2021.102358

Zolkos, S. G., Goetz, S. J., & Dubayah, R. (2013). A meta-analysis of terrestrial aboveground biomass estimation using lidar remote sensing. *Remote Sensing of Environment*, *128*, 289–298. https://doi.org/10.1016/j.rse.2012.10.017